Bimetallic Ni-Zn/TiO2 catalysts for selective hydrogenation of alkyne and alkadiene impurities from alkenes stream

Zhao Wang, Guillaume Wang, Catherine Louis, Laurent Delannoy

Bimetallic Ni-Zn/TiO_2 catalysts for selective hydrogenation of alkyne and alkadiene impurities from alkenes stream

Zhao Wang[1,3], Guillaume Wang[2], Catherine Louis[1], Laurent Delannoy[1*]

1- Sorbonne Université, CNRS, Laboratoire de Réactivité de Surface, LRS, F-75252 Paris, France.

2- Université Paris Diderot, Sorbonne Paris Cité, CNRS, Laboratoire Matériaux et Phénomènes Quantiques, UMR 7162, 75013, Paris, France.

3- Present address: State Key Laboratory Advance Technology for Materials Synthesis and Processing, School of Materials Science and Engineering, Wuhan University of Technology, 122, Luoshi Road, Wuhan, 430070, China.

Running title: Bimetallic Ni-Zn/TiO_2 catalysts for selective hydrogenation of alkyne and alkadiene impurities from alkenes stream.

* To whom correspondence should be addressed:

E-mail: laurent.delannoy@sorbonne-universite.fr

Keywords: Deposition-precipitation, Ni-Zn/TiO_2, Nanoalloy, Bimetallic catalysts, Selective hydrogenation.

ABSTRACT

This study investigates the alternative of replacing noble metals by base metals as catalysts for selective hydrogenation of polyunsaturated hydrocarbons. Nickel catalysts are active for this type of reaction, but poorly selective. However, former calculations anticipated that Ni-Zn alloys could have higher selectivity to alkenes than monometallic Ni depending on the Ni/Zn atomic ratio in the alloy. In this contribution, Ni-Zn alloy nanoparticles supported on TiO_2 are synthesized as catalysts for selective hydrogenation of acetylene and butadiene. The designed catalysts with 0.5 wt% Ni loading and various Ni/Zn nominal ratios are prepared by deposition-precipitation with urea (DPU). STEM-HAADF imaging coupled with EDS analysis reveals that Ni-Zn bimetallic particles are formed after reduction treatment at 450 °C. Alloying Ni with Zn leads to a slight increase of the average particle size and a broadening of the size distribution compared to monometallic Ni. However, the average Ni/Zn atomic ratio measured by EDS in the bimetallic particles is always higher than the nominal one, which could be due to Zn evaporation under the beam. The results of acetylene hydrogenation show that although the catalytic activity is slightly reduced after alloying Ni with Zn, the selectivity to ethylene is enhanced from 50% up to 85%, at the expense of the formation of oligomers (coupling products). However, the bimetallic Ni-Zn catalysts suffer from progressive deactivation in this reaction. During butadiene hydrogenation performed in the presence of an excess of propene, the bimetallic Ni-Zn/TiO_2 catalysts are significantly more stable, with a high and constant selectivity to butenes (>95%), compared with Ni/TiO_2, which deactivates rapidly in the first hours. Some hypotheses concerning the observed differences in catalytic stability are discussed.

INTRODUCTION

Light alkenes resulting from steam cracking of petroleum alkanes are required to have high purity for industrial polymer synthesis as the alkynes and alkadienes impurities contained in these alkenes streams can poison the catalysts used for the polymerization reactions [1]. For instance, the acetylene concentration in ethylene stream must be controlled to be less than 5 ppm for the synthesis of polymer grade ethylene [2], and methyl acetylene-propadiene (MAPD) is only tolerable at concentration lower than 1 ppm in the polymer grade propylene [3]. Considering the high amount of alkynes and alkadienes impurities in raw light alkenes steams, for instance 2.0 to 8.0% of propyne and propadiene in propene [4] and 0.3 to 6.0% of residual butadiene in butenes [5, 6], these impurities must be eliminated before the polymerization process. Currently, catalytic semi-hydrogenation is the main way to reduce the impurities by transforming them to light alkenes without over-hydrogenation to alkanes or formation of oligomers.

Palladium-based catalysts, e.g., Pd/Al_2O_3 with low metal loading (ca. 0.3 wt %), prepared by impregnation and commercialized by Sud-Chemie [7, 8] have been recognized as one of the best catalysts for industrial semi-hydrogenation reactions. Even though monometallic palladium catalysts have high activity, their selectivity to alkenes decreases dramatically at high alkyne or alkadiene conversion. For instance, the selectivity to ethylene decreases from 90 to 10% when acetylene conversion increases from 80 to 100% for selective acetylene hydrogenation in excess of ethylene on 3 wt% Pd/ boehmite catalyst [9]. Thus, palladium-based catalysts are usually modified either by inclusion of carbon, sulfur, co-feeding with CO [10-12], or alloying with a second metal, e.g., Pd-Pt or Pd-Ag [9, 13-16]. It was found that the addition of a second metal could prevent the diffusion of hydrogen into the metal subsurface [17] and thus hinder over-hydrogenation [18]. In addition to the selectivity, the cost of the catalysts is also of great importance for practical applications. Typically, this cost can be

reduced either by lowering the noble metal loading in the catalysts or by developing new non-noble metals catalysts. In the last decade, several approaches have been explored in the literature [19]. One approach is to nanostructure less conventional metals than Pd, such as Au and Ag, to create large amount of surface defects, which can promote H_2 activation. The other one is to alloy palladium with other metals (e.g., Ag, Cu, Zn, Ga) to provide controlled ensembles of atoms and/or to modify the electronic properties of the active sites for adsorption of reactants and products [20, 21]. In the hydrogenation of butadiene, Al_2O_3-supported Pd-Ni alloy catalysts show a higher catalytic activity and selectivity to 1-butene than palladium catalysts as alloying with Ni decreases the activation barrier for hydrogenation and the 1-butene binding energy [22]. In acetylene hydrogenation, bimetallic Pd-Cu catalysts have lower activity but higher stability than palladium catalysts because the addition of copper reduces the reaction of oligomerization (green oil formation and accumulation) by decreasing multiple Pd sites for adsorption of acetylene [23]. Other Pd-based catalysts, such as Pd-Pt catalysts (BASF NanoSelect^{TM} catalysts), were developed using colloidal deposition method and showed higher performance than the classical Lindlar's catalysts (Pd catalysts modified by lead or sulfur) in liquid phase selective hydrogenation reactions [24]. However, the high cost of Pd-based catalysts is still a concern and it would be very interesting and valuable to replace palladium by low cost non-noble metal elements.

Through density functional theory calculations (DFT), Studt et al [25] proposed that some non-noble bimetallic catalysts, such as Cu-Zn, Fe-Zn and Ni-Zn, could be valuable alternatives to palladium ones. Our group has recently experimentally verified that supported bimetallic Cu-Zn nanoparticles have high activity and selectivity as well as higher stability in selective hydrogenation of butadiene than monometallic Cu as the interaction with Zn decreases oligomers formation on the catalyst surface [26]. In the article mentioned above [25], experimental results showed that the addition of Zn to Ni/$MgAl_2O_4$ with a Ni/Zn ratio of 1/3

resulted in the formation of a lower amount of ethane than monometallic Ni catalyst during selective hydrogenation of acetylene, but no evidence of Ni-Zn alloy formation was reported, and the Ni-Zn catalysts stability was not studied. More recently, Spanjers et al [27] studied bulk intermetallic Ni-Zn compounds (Ni_4Zn_1, Ni_1Zn_1 and Ni_5Zn_{21} alloys) for selective acetylene hydrogenation in excess of ethylene and found that zinc inclusion into nickel could reduce the oligomerization reaction, leading to higher selectivity to ethylene. To extend the study to supported nanoparticles, they carried another work on Ni/ZnO and Ni/SiO_2 catalysts [28] and found that Ni-Zn nano-alloys (α-NiZn (Ni_4Zn) or β-NiZn (Ni_1Zn_1) depending on the sample reduction temperature) were formed directly in Ni/ZnO sample after reduction at temperature higher than 300 ºC, without any monometallic Ni particle formation. However, they found that Ni/ZnO catalysts displayed a lower selectivity to ethylene than Ni/SiO_2 as a result of oligomerization reactions occurring on the ZnO support, and they concluded that the ZnO support had a negative effect on ethylene selectivity. In addition, Ni-based catalysts have also been explored by adding other elements, e.g., Cu [29], Fe [30], B and P [31-33] for selective hydrogenation reactions. Liu et al [34] also found that unsupported intermetallics Ni_xM_y (M=Ga, Sn) have excellent selectivity toward alkenes and good stability during long-term acetylene hydrogenation. A promotional effect of Indium in Ni_xIn/SiO_2 catalysts for some specific Ni/In ratios on acetylene conversion, ethylene selectivity and catalyst stability was also observed [35].

Since the Ni-Zn catalysts could present interesting catalytic performances [25], it was valuable and interesting to explore the preparation of bimetallic Ni-Zn catalysts supported on another support than ZnO. Our choice went to TiO_2, which has stable surface at low reduction temperature [36] and no catalytic activity for hydrogenation reaction. In this work, TiO_2 supported Ni-Zn catalysts are prepared by deposition-precipitation with urea (DPU). They are deeply characterized and the catalytic performances including activity, selectivity, and stability

are evaluated in the hydrogenation of pure acetylene in the one hand and the selective hydrogenation of butadiene in the presence of an excess of propene in the other hand.

1. EXPERIMENTAL SECTION

1.1 Catalysts preparation

Monometallic Ni/TiO_2 and bimetallic Ni-Zn/TiO_2 catalysts were prepared using the method of deposition-precipitation with urea (DPU) as described previously [37-39] to reach a nickel loading of 0.5wt%. Briefly, after filling a double wall reactor with 300 ml of distilled water, 3 g of support (TiO_2 P25 Evonik, 80% anatase and 20% rutile, 50 m^2 g^{-1}) were added. The reactor was heated to 80 ºC by a water heating system. Then, an appropriate amount of $Ni(NO_3)_2 \cdot 6H_2O$ and/or $Zn(NO_3)_2 \cdot 6H_2O$ precursors was added into the reactor to achieve the desired nominal nickel and zinc loadings (0.5 wt% Ni loading with Ni:Zn atomic ratios of 1:0, 1:1, 1:3 and 1:5, the samples will be labelled Ni, NiZn1, NiZn3 and NiZn5 respectively). Meanwhile, urea was added to achieve a urea to metal molar ratio of 100. The mixture was kept at 80 °C in the closed reactor for 20 h under continuous stirring. The solids were finally separated from the liquid by centrifugation and subsequently washed with distilled water and centrifuged (three times). All the samples were further dried under vacuum at room temperature (RT) for 24 h (as-prepared sample).

Before characterization or catalytic reaction, the as-prepared samples were calcined at 400 °C for 2 h after sample heating with a rate of 5 °C min^{-1}, under flowing air (100 mL min^{-1}), then reduced at 450 °C for 2 h with a heating rate of 3 °C min^{-1}, under flowing pure H_2 (100 mL min^{-1}).

2.2 Instrumentation and measurements

The metals loadings in each sample were detected by X-ray fluorescence (XRF) with a spectrometer XEPOS HE (AMETEK). The method used for the XRF analyses is based on calibration curves obtained from standards for each element.

The reduction of the calcined samples was followed by temperature programmed reduction (TPR), which was performed on a Micromeritics Autochem II Automated Catalyst Characterization System under 5% H_2/Ar gas mixture (25 mL min^{-1}). 100 mg of catalyst was filled into the reactor and the hydrogen consumption was recorded during temperature increase from RT to 550 ºC with a heating rate of 7.5 °C min^{-1}. H_2 consumption for Ni^{2+} ions reduction was calibrated using 100 mg of pure NiO as a reference.

XRD analysis was performed on the reduced samples with a diffractometer (D8 Bruker Company) using the Cu Kα radiation (1.5418 Å; 40 kV and 30 mA) with a Ni filter under air. The crystallite sizes were calculated using Scherrer's equation [40], and correction for instrumental broadening was applied. In the diffractograms, the (200) peak of anatase TiO_2 at $2\theta = 48.1$ was used as a reference to determine the position of the diffraction peaks of nickel-containing compounds as it does not interfere with any of them.

Scanning and transmission electron microscopy with high-angle annular dark-field (STEM-HAADF) and energy-dispersive X-ray spectroscopy (EDS) were used to identify the size and compositions of the metal nanoparticles. This was performed with a JEOL ARM 200F microscope, equipped with a cold field emission gun and a CEOS aberration corrector of the objective lens, operated at 200 kV [41]. Statistical analysis of the metal particle size distribution (PSD) in reduced samples was obtained by counting more than 200 particles, using the software Image J. The average particle diameter was deduced from the formula $d_m = \sum n_i d_i^3 / \sum n_i d_i^2$, where n_i is the number of the particles of diameter d_i. The detection limit of the particles was 0.5 nm at 200 kV. The average particle sizes were measured from STEM-HAADF assuming

spherical shapes and the mean Ni/Zn atomic ratios were obtained from the EDS analyses of a set of individual particles.

After some specific catalytic tests, thermogravimetric analysis (TG) of the catalysts was performed using a Seiko 320 thermobalance. Around 20 mg of catalysts were heated under air (100 ml min^{-1}) from room temperature to 900 ºC with a heating rate of 5 ºC min^{-1}.

2.3 Acetylene and Butadiene selective hydrogenation reactions

The reaction of acetylene hydrogenation was carried out with 200 mg of a mixture containing 50 mg of catalysts (0.5 wt% Ni and various Ni/Zn ratios) and 150 mg of SiC in a plug-flow microreactor (4 mm of internal diameter). The particle size of powder of both catalysts and SiC support was controlled by sieving between 125 and 200 μm. The *ex situ* calcined catalysts were activated *in situ* under pure H_2 (100 mL min^{-1}) from RT to 450 °C (3 °C min^{-1}) then 2 h at 450 °C. After activation and cooling down to 100 °C under H_2, the reaction mixture consisting of 2% acetylene and 20% hydrogen in He was introduced with a total flow rate of 100 mL min^{-1}, which corresponded to a space velocity of 30 L g^{-1} h^{-1}. The reaction temperature was then increased at the rate of 1°C/min from 100 °C to a final temperature between 165-175°C depending on the catalyst, in order to achieve an acetylene conversion in the range 90-98%. The reaction was maintained at the final temperature for about 20h in order to monitor the stability of the catalysts. Gas Chromatography (GC) analysis of the reaction reactant and products (acetylene, ethylene, ethane) was performed using a micro-GC Varian 4900 every 10 min. The formation of C-C coupling products (oligomers) was not detected by GC but the selectivity to such oligomers was calculated on the basis of the mole balance between the amount of acetylene consumed and the one of ethylene and ethane produced (see supplementary information).

The reaction of butadiene hydrogenation in an excess of propene was carried out on 100

mg of a mixture containing 10 mg of catalysts (0.5 wt% Ni with various Ni/Zn ratios) and 90 mg of pure TiO_2 support (sieve fraction, 125-200 μm) in a plug flow microreactor (4 mm of internal diameter), either for temperature-programmed reaction or for isothermal reaction. The *ex situ* calcined catalysts were activated *in situ*, under pure H_2 (100 mL min^{-1}) from RT to 450 °C (3 °C min^{-1}) then held for 2 h at the final temperature. After cooling down to room temperature under H_2, the reactor was immersed into a water bath connected to a temperature controller and the reaction mixture consisting of 0.3% butadiene, 30% propene and 20% hydrogen in He was introduced with a total flow rate of 50 mL min^{-1}, which corresponded to a space velocity of 30 L g^{-1} h^{-1} (GHSV = 20,000 h^{-1}).

In the case of the temperature-programmed reaction, the analysis of the reaction mixture at the outlet of the reactor was done every 5 ºC from 10 °C to 80 °C after stabilization at each temperature for 15 min. The analysis of the reaction products was performed by gas chromatography (Perichrom PR 2100, FID detector). In the case of the isothermal reaction, after *in situ* reduction at 450 ºC for 2 h, the reactor was also immersed into the water bath at a given temperature, and the reaction was performed during 20 h. It was monitored at a specific reaction temperature, to provide a similar initial butadiene conversion around 90% for all the catalysts, with a GC analysis performed every 15 min. As mentioned in [42], tests were made to attest that under the catalytic conditions described and at low conversion, internal and external diffusion limitations could be neglected.

The detailed calculations of the conversions, selectivities for the various reactants and products, concentration in alkanes, activities and TOF can be found in the supplementary information.

2. RESULTS AND DISCUSSION

3.1 Samples characterization

The metals loadings in the as-prepared Ni and Ni-Zn samples are summarized in Table 1, which shows that the final Ni loadings are close to the nominal ones while the Zn loadings are always slightly lower than the nominal ones.

Table 1: Experimental metal loadings in the Ni-Zn/TiO_2 samples prepared by DPU determined by XRF and composition of the NiZn /bimetallic particles in Ni-Zn/TiO_2 determined by EDS.

Catalysts	Nominal loadings		Experimental loadings for as-prepared samples			Experimental loadings after reduction under H_2 at 450 °C			Average Ni/Zn atomic ratios in nanoparticles from EDS
	Zn (wt%)	Ni (wt%)	Zn (wt%)	Ni (wt%)	Ni/ Zn atomic ratios	Zn (wt%)	Ni (wt%)	Ni/Zn atomic ratios	
Ni	-	0.5	-	0.54	-		0.54		-
NiZn1	0.5	0.5	0.45	0.57	1.4	0.37	0.56	1.7	12
NiZn3	1.5	0.5	1.35	0.6	0.5	1.02	0.61	0.7	3.3
NiZn5	2.5	0.5	2.30	0.65	0.3	1.33	0.65	0.55	1.8

The temperature for the reduction of calcined Ni-Zn/TiO_2 was selected according to the results of temperature programmed reduction under H_2 (TPR-H_2) presented in Figure 1. For comparison, TPR of calcined 0.5 wt% Zn/TiO_2 is also included in Figure 1 and shows no reduction peaks in the range 50-550 °C. The maximum temperature for TPR was set at 550 °C to avoid the contamination of the TPR equipment with volatile Zn^o [43-46]. For the Ni/TiO_2 sample, two reduction peaks can be observed at about 400 ^{o}C and 530 ^{o}C, similar to previous TPR results on Ni/TiO_2 samples prepared by $[Ni(NH_3)_6]^{2+}$ adsorption [47]. For the Ni-Zn/TiO_2 samples, the reduction temperatures shift to higher values with increasing Zn loading, leaving only the low reduction temperature peak visible. To verify whether all the Ni^{2+} ions were reduced in the low temperature range (350-475 ^{o}C), the percentage of Ni^{2+} reduction in the first reduction peak of the sample was calculated by using the TPR of pristine NiO as a reference and the results are summarized in Table S1. It appears that almost all the Ni^{2+} species were

reduced to metallic Ni in the temperature range below 500 °C. As a consequence, the high temperature peak observed for Ni/TiO_2 probably corresponds to the reduction of TiO_2 support, as reported by Geus et al. [48] who found that the total hydrogen consumption was larger than that required for full reduction of nickel ions in Ni/TiO_2 samples reduced up to 900 ºC. Based on Figure 1, a temperature of 450 ºC with a 2h-plateau was selected for sample activation before characterisation and catalytic reaction. Considering the low melting temperature of metallic Zn (420 ºC), the metal loadings were also determined by XRF after reduction at 450 °C. Table 1 shows a noticeable decrease of the zinc content, that can be related to the partial evaporation of this element in such a temperature and pressure range [49, 50]. Similar Zn decreases was also observed and discussed during the reduction Cu-Zn catalysts in a former paper [26]. Therefore, the Ni/Zn ratios obtained after the reduction treatment are significantly higher than the nominal ones.

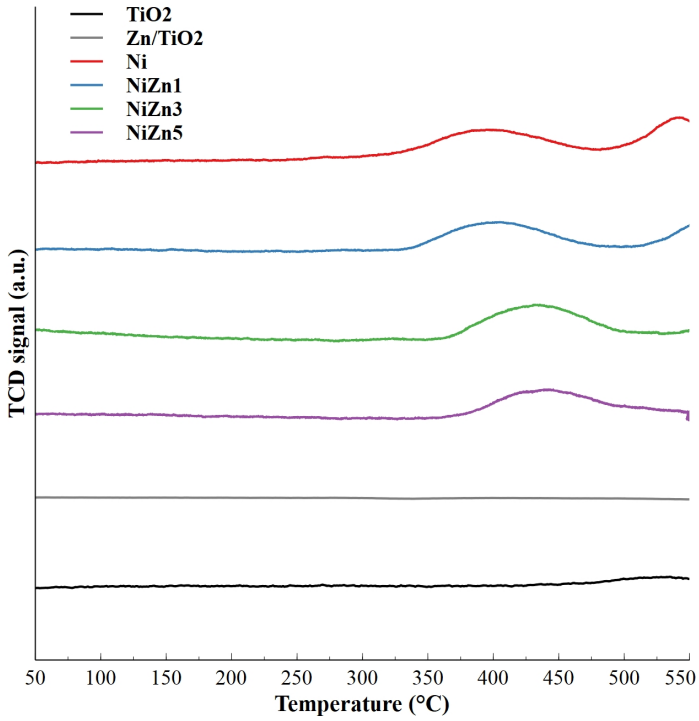

Figure 1. TPR of calcined Ni/TiO_2, Zn/TiO_2 and Ni-Zn/TiO2 catalysts with bare TiO_2 as a reference

Figure 2 shows the XRD patterns of 0.5 wt% Ni-Zn/TiO_2 samples in the range 40-46° after calcination at 400 °C, followed by reduction at 450 °C. It is not clearly different from the XRD diagram of TiO_2 support plotted on the same figure. Only the NiZn5 sample shows an additional peak (43.3°) to the ones of the support. It is significantly shifted from the main peak of metallic Ni expected at 44.5° (JCPDS: #71-4655), and corresponds to the one of Ni-Zn alloy (43.3° JCPDS card: # 72-2668). According to the information given on the JCPDS card and the relationship between the crystal lattice spacing and the composition of Ni-Zn alloy [51], the Ni-Zn alloy seems to correspond to β_1-NiZn alloy with 50 at% Ni (Ni_1Zn_1 alloy). Using the Scherrer's equation, the Ni-Zn alloy crystallite size was estimated to be about 6 nm for NiZn5 but the margin of error on this value is high due to the weak intensity of the peak. For the other Ni-Zn/TiO_2 samples, the crystallite size of metallic Ni or Ni-Zn phase may be too small to be detected by XRD, or the peak could overlap with the broad TiO_2 peak at 44°.

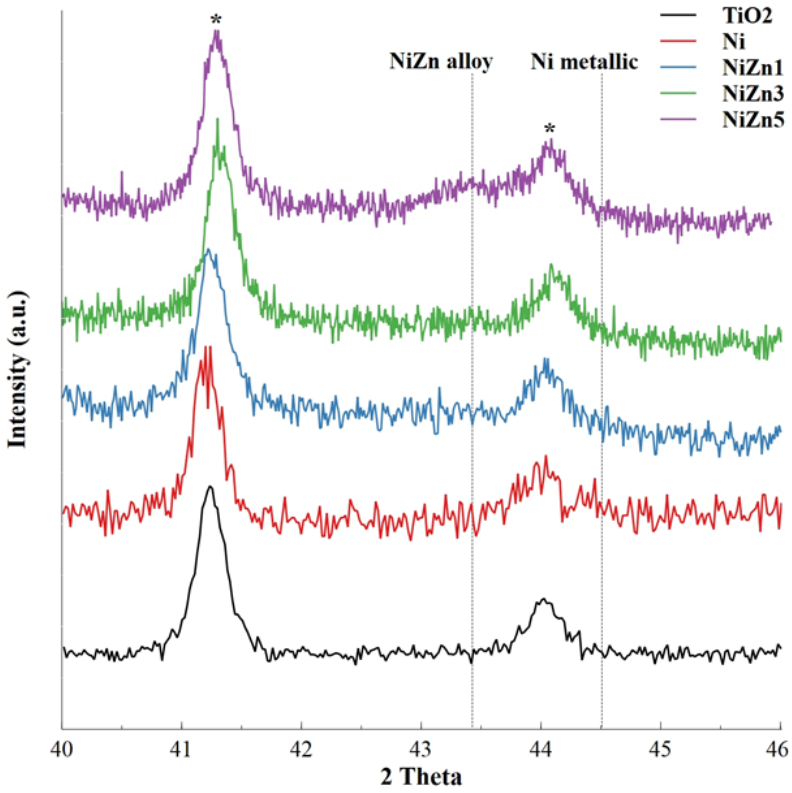

Figure 2. XRD patterns of the calcined-reduced Ni-Zn/TiO_2 samples (0.5 wt% Ni) with bare TiO_2 as a reference. * Rutile TiO_2 (JCPDS: 01-086-0147); NiZn alloy peak position from JCPDS: 01-072-2668; metallic Ni peak position from JCPDS: 00-004-0850

The various samples prepared with 0.5 wt% Ni were imaged by STEM-HAADF after calcination at 400 °C then reduction at 450 °C (Figure 3). The average particle size deduced from the particle size distribution is included in Table 2. For the 0.5 wt% Ni/TiO_2 sample (Figure 3a), small particles are visible with an average particle size of 3.2 nm. The particle size slightly increases when Zn is present to 3.4, 3.8 and 4.1 nm for the NiZn1, NiZn3 and NiZn5 samples, respectively and the addition of Zn also broadens the size distribution in the Ni-Zn/TiO_2 samples (Figure 3b-d). For instance, the particles size distribution is in the range of 1 to 6 nm for NiZn1 whereas it is of 1 to 9 nm for NiZn5.

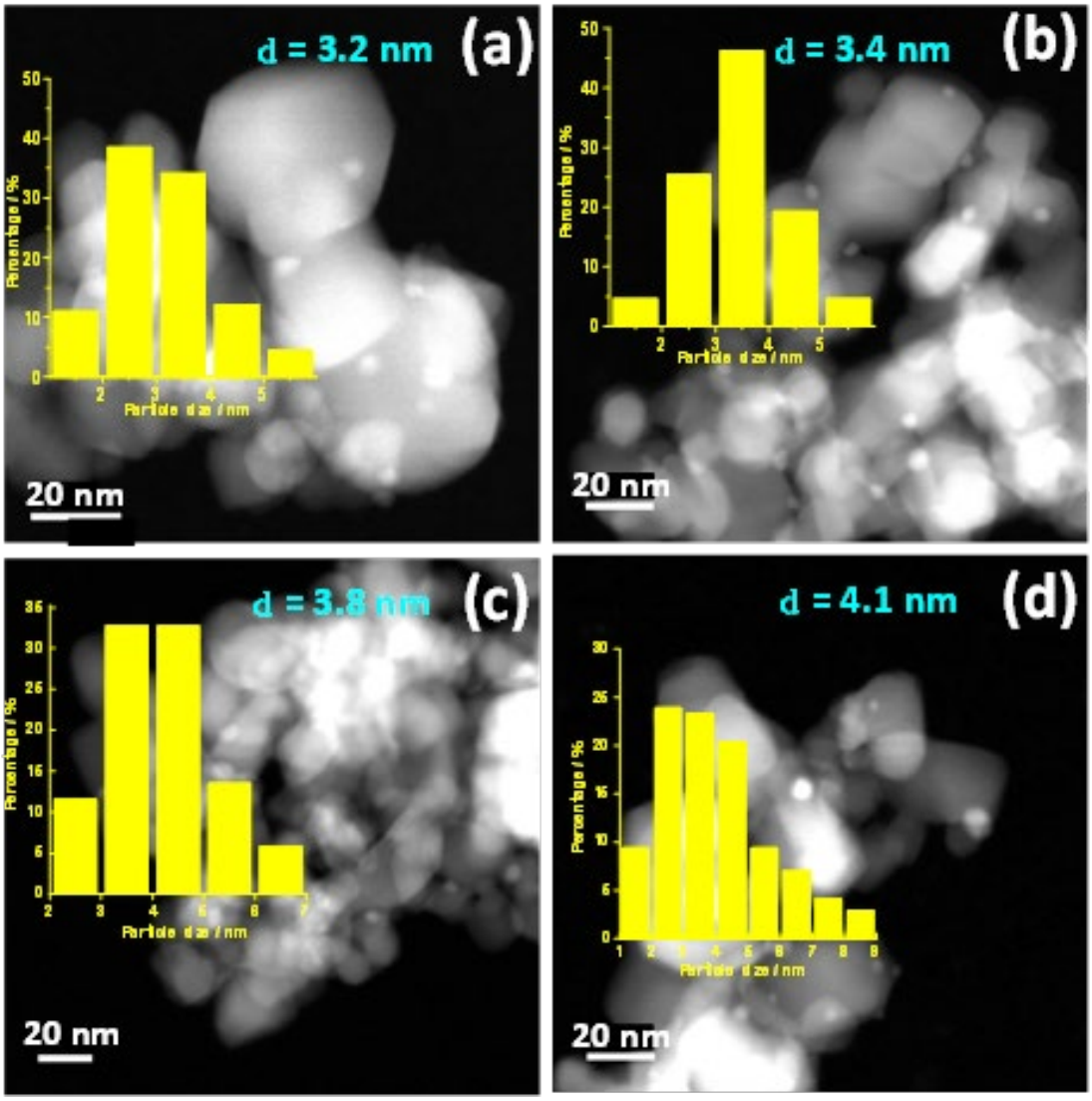

Figure 3. STEM-HAADF images of the calcined-reduced Ni-Zn/TiO_2 samples (0.5 wt% Ni) with the particle size distribution: Ni (a); NiZn1 (b); NiZn3 (c); NiZn5 (d)

Table 2: Size of the NiZn /bimetallic particles in Ni-Zn/TiO_2,(0.5 wt% Ni) determined by electron microscopy and catalytic activity and TOF in acetylene hydrogenation and butadiene selective hydrogenation in excess of propene.

Sample	Average metal particle size (nm, based on TEM)	Acetylene hydrogenation		Butadiene selective hydrogenation in excess of propene	
		Activity at 130 °C ($\times 10^{-4}$ $mol_{acetylene}$ s^{-1} g_{Ni}^{-1})	TOF at 130 °C (s^{-1}) [b]	Activity at 20 °C ($\times 10^{-4}$ $mol_{butadiene}$ s^{-1} g_{Ni}^{-1})	TOF at 20 °C (s^{-1}) [b]
Ni	3.2	26	0.5	16	0.3
NiZn1	3.4	16	0.5	9	0.3
NiZn3	3.8	12	0.75	10	0.6
NiZn5	4.1 / 5.8[a]	12	0.9	4	0.25

[a]: crystallite size estimated from XRD
[b]: all the metal particles are assumed as spherical shape

Since Ni-Zn alloy formation was only detected by XRD for NiZn5, STEM-HAADF coupled with Energy Dispersive X-ray spectrometry (EDS) was performed on a series of individual particles in the three Ni-Zn/TiO_2 samples to determine the Ni/Zn atomic ratios as a function of the nanoparticle size. The EDS results in Figure 4 show that Ni-Zn alloys are formed in all the particles analysed for the three samples and that the Ni/Zn atomic ratio increases with the decrease in particle size in each of the Ni-Zn/TiO_2 samples. The average Ni/Zn atomic ratios decrease with increasing Zn loading from 12 in NiZn1 (Ni/Zn=1.69 after reduction at 450 °C) to 1.8 in NiZn5 (Ni/Zn=0.54 after reduction) (Table 1). It is worth to note that the composition of the Ni-Zn nanoparticles determined by EDS suggests that only a fraction of zinc present in the samples is alloyed with nickel, implying that another fraction might be present on the support surface. The nature of these residual Zn species is unknown, the presence of ZnO being

not evidenced by XRD (Figure S1). However, it is also possible that Zn sublimates under exposure to the electron beam during the EDS analysis as previously proposed for carbon supported Pd-Zn bimetallic particles [52], which may result in a strong underestimation of the Zn content.

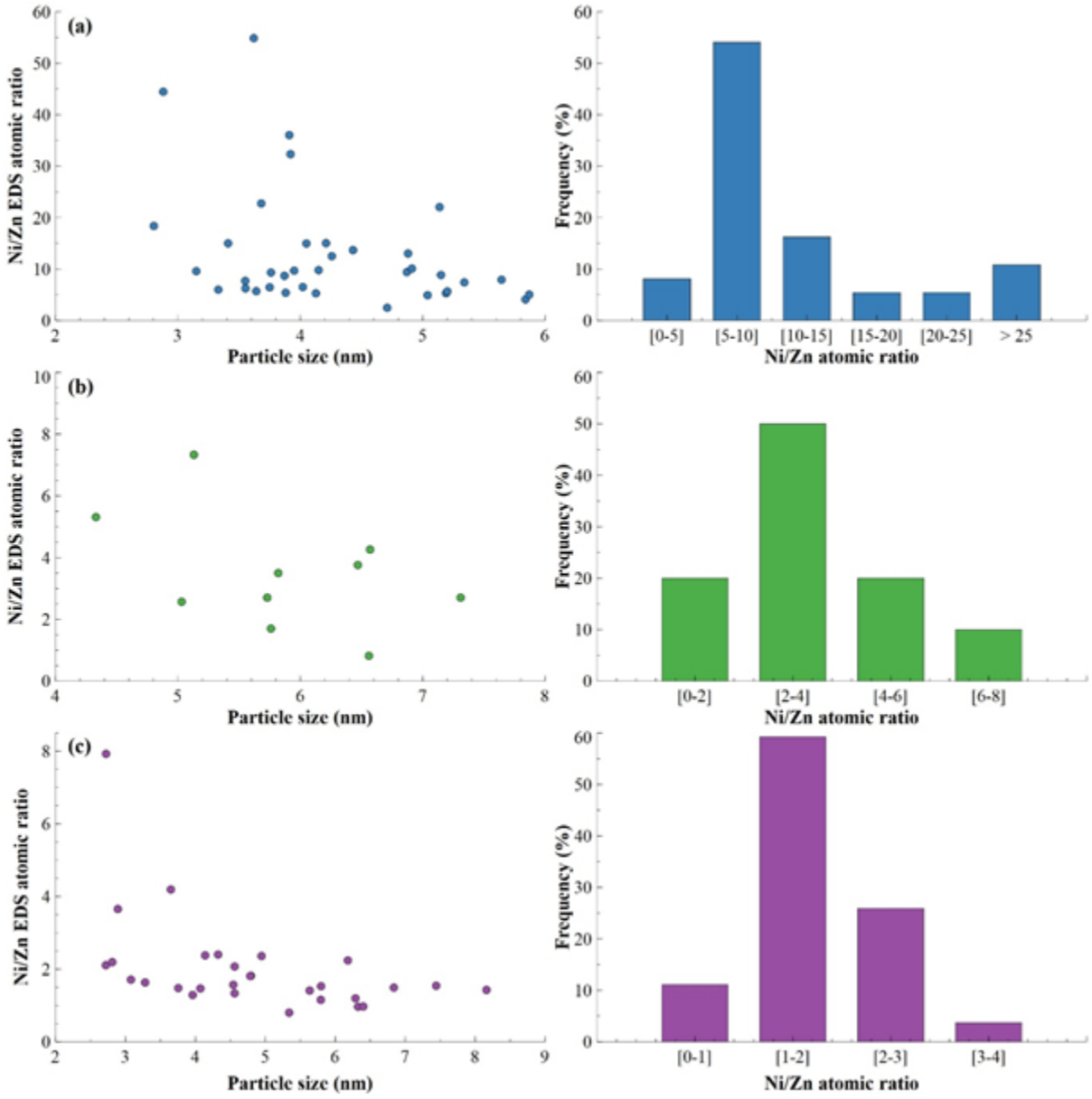

Figure 4. Ni/Zn atomic ratio determined by EDS analysis as a function of particle size (left panel) and Ni/Zn atomic ratio distribution (right panel) for the calcined-reduced Ni-Zn/TiO_2 samples (0.5 wt% Ni): NiZn1 (a); NiZn3 (b); NiZn5 (c)

3.2 Hydrogenation of pure acetylene and hydrogenation of butadiene in an excess of propene

3.2.1 Hydrogenation of pure acetylene

The hydrogenation of acetylene was studied in the absence of an excess of alkene, examining the selectivity to ethylene, ethane and oligomers, first by temperature programmed reaction from 100 °C to 165-175°C (range of temperature allowing to reach 90-98% acetylene conversion for all the catalysts). The final temperature was then kept constant for about 24h in order to evaluate the stability of the Ni and NiZn samples. One can remind that the catalytic beds contain the same mass of Ni. Zn(2.5 wt%)/TiO_2 does not present any activity in the temperature range 100-200 °C (not shown).

Figure 5a and Table 2 shows that the Ni/TiO_2 catalyst is the most active catalyst and that the addition of Zn decreases the acetylene conversion. NiZn3 is the least active one among the bimetallic catalysts. However, the TOF values calculated at 130 °C seems to indicate that nickel in the bimetallic Ni-Zn catalysts is more active than in the monometallic Ni/TiO_2, provided that the values are meaningful (see supplementary information for detailed calculations and hypotheses). The evolution of the selectivity to ethylene and ethane as a function of the acetylene conversion, reported in Figures 5b and 5c, shows that the selectivity to both products is rather constant up to a C_2H_2 conversion of 80%, the bimetallic Ni-Zn catalysts being clearly more selective to ethylene (70-80%) than Ni (less than 50%) (Figure 5b). At acetylene conversion higher than 80%, the selectivity to ethane starts to increase, especially for NiZn1 (Figure 5c). The monometallic Ni catalyst has a high selectivity to oligomers (above 40%) whatever the C_2H_2 conversion whereas the oligomers formation continuously decreases for all the bimetallic catalysts (Figure S2).

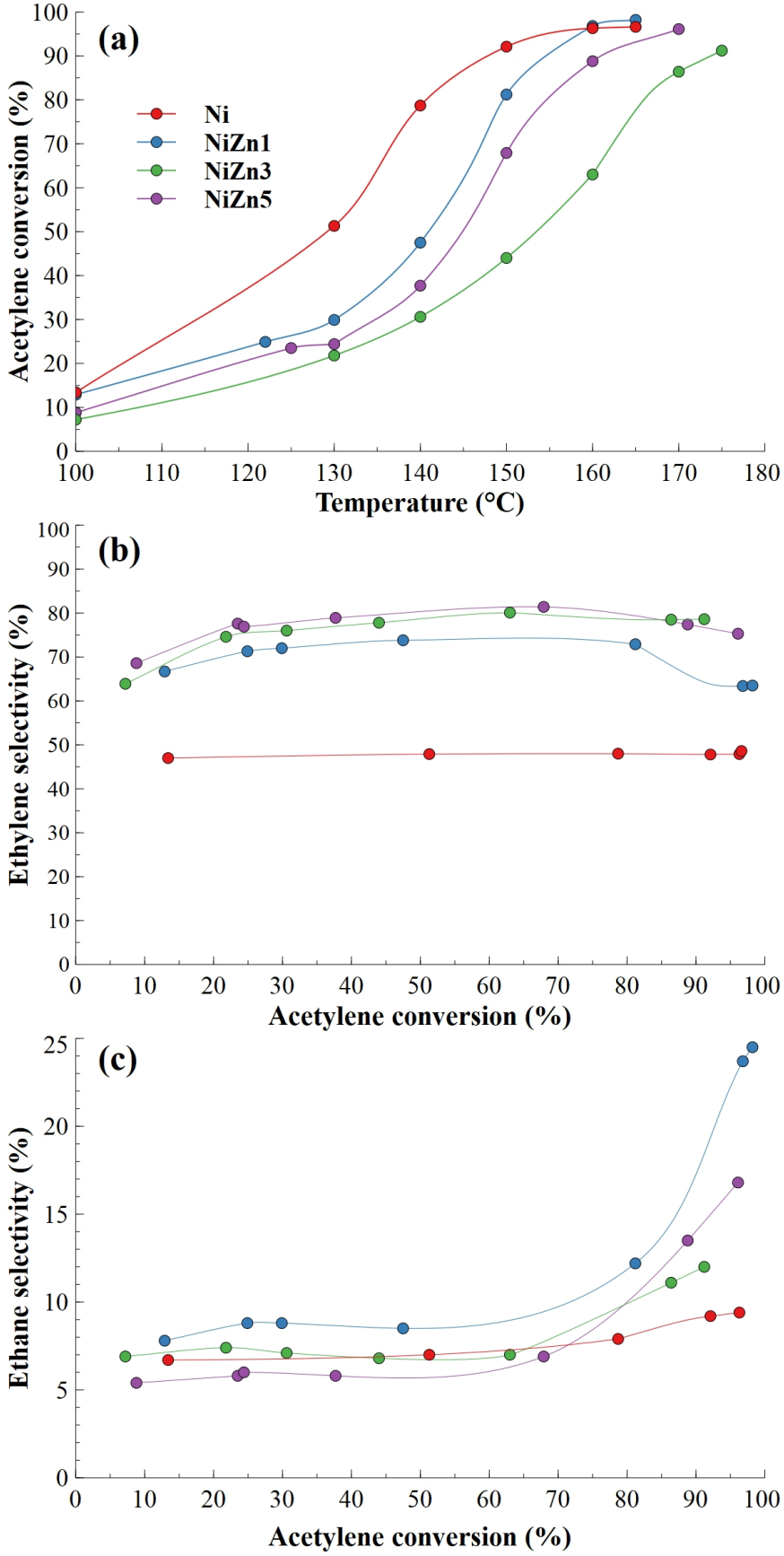

Figure 5. Evolution of the acetylene conversion with reaction temperature (a) and evolution of the selectivity to ethylene (b) and ethane (c) as a function of acetylene conversion during temperature programmed reaction of acetylene hydrogenation for the calcined then reduced Ni and Ni-Zn/TiO_2 catalysts (0.5 wt% Ni) (50 mg of catalyst diluted with 150 mg SiC).

After reaching an acetylene conversion in the range 90-98% for all the samples, the stability of the catalysts was monitored with time on stream at constant temperature (between 165 and 175 °C, depending on the catalyst) (Figure 6a). The monometallic Ni/TiO_2 is the most stable catalyst, with a C_2H_2 conversion above 80% even after 22h of reaction. Bimetallic NiZn1 and NiZn3 samples deactivate with time in a similar way, with a sensible loss of conversion in the first 10h on stream before continuing with a slow decrease of conversion with time. NiZn5 shows a different profile of deactivation with slower initial but continuous and almost linear loss of activity with time. Given the relatively low reaction temperatures used, the hypothesis of particle sintering during the reaction can be discarded to explain the observed deactivations. Regarding the selectivity, Figure 6b presents the evolution of the selectivity to ethylene with time on stream for the whole experiments. It is interesting to note that the selectivity to C_2H_4 remains nearly constant for all the catalysts above 5h reaction, even the ones that significantly deactivate. The same trends are observed for the selectivity to ethane and oligomers (Figure S3). It also appears that the addition of Zn to Ni increases the selectivity to ethylene, with an effect more marked for the catalyst containing the higher amount of Zn. Figure 6c presents the average selectivities to ethylene, ethane and oligomers calculated between 5 and 22h of reaction for all the catalysts. The increasing selectivity to ethylene from about 55% for Ni/TiO_2 up to 75-85% for the $Ni\text{-}Zn/TiO_2$ catalysts is essentially at the expense of the one to oligomers as the selectivity to ethane is almost equivalent and remains around 8-9% for all the catalysts.

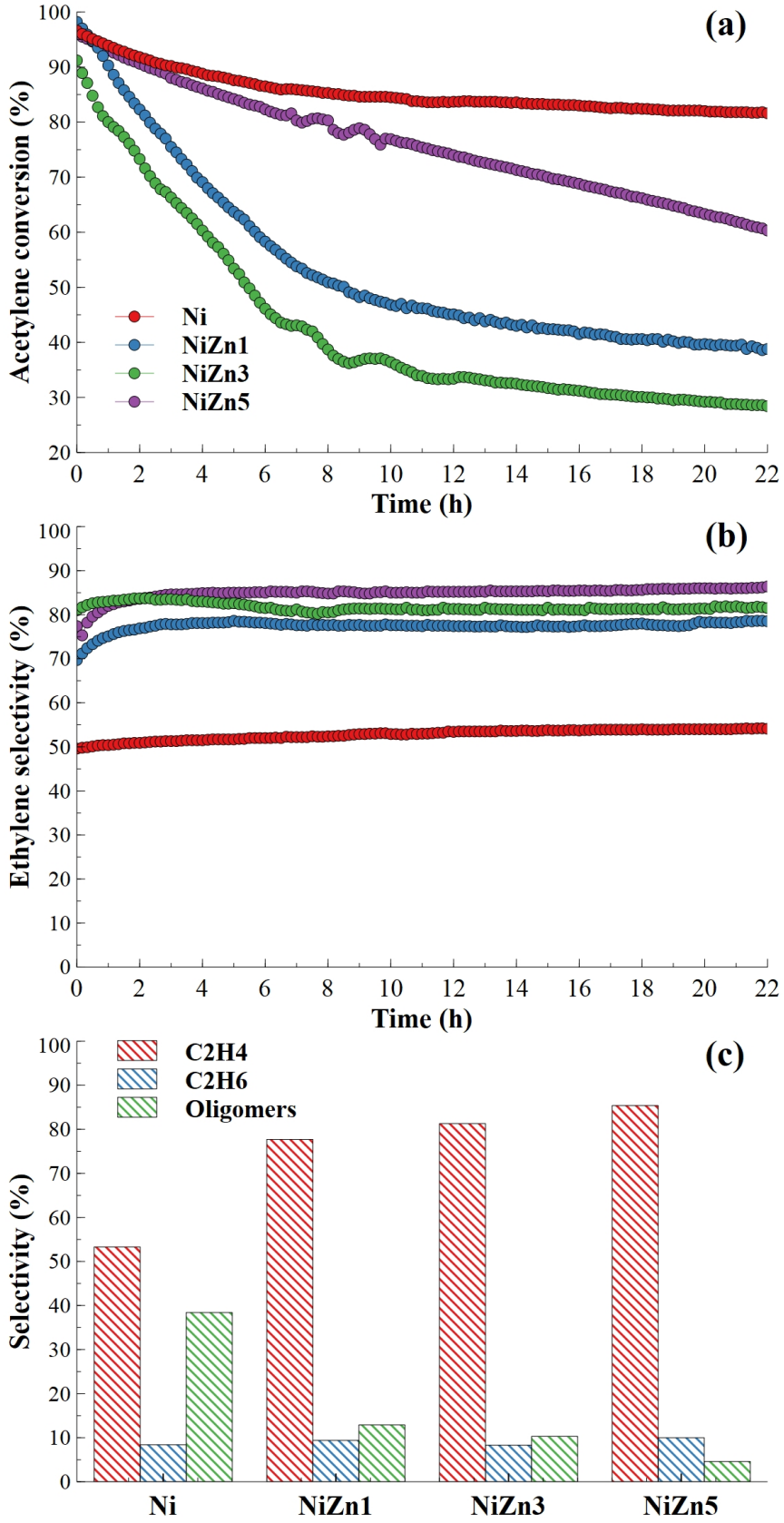

Figure 6. Evolution of the acetylene conversion (a) and the selectivity to ethylene (b) during acetylene hydrogenation with time on stream at 165 °C for Ni and NiZn1, 175 °C for NiZn3 and 170 °C for NiZn5. Average selectivities to ethylene, ethane and oligomers at pseudo-stable state (c) for the calcined then reduced Ni and Ni-Zn/TiO_2 catalysts (0.5 wt% Ni) (50 mg of catalyst diluted with 150 mg SiC).

The lower activity of the Zn-containing catalysts compared to the Ni counterparts is in line with what was previously observed for Ni-Zn systems in selective hydrogenation reactions [27, 53]. For acetylene hydrogenation, such a decrease in activity was ascribed to the lower acetylene adsorption energy on Ni-Zn intermetallic compounds [27], which results from the substitution of Ni atoms by Zn ones at the surface of the bimetallic nanoparticles. Ni substitution by a second metal, such as Zn [25] and Pt [54], was proposed to modify the electronic properties of surface Ni atoms and thus the strength of adsorption of reactants [55]. It was also proposed recently that the Zn atoms prefer to replace the Ni atoms at low coordination sites (corners, edges or defects) of the particles surface [56, 57]. As the low coordination Ni sites are expected to bind unsaturated compounds more strongly than terrace sites [58], their replacement by Zn atoms could also contribute to lower the activity of bimetallic samples.

In the case of selective hydrogenation of acetylene in the presence of ethylene over bulk intermetallic Ni-Zn compounds in a batch reactor [27], the formation of Ni-Zn alloys was also shown to result in a decrease in the oligomers formation and in an enhancement of the selectivity to ethylene. The lower acetylene adsorption energy, estimated from DFT calculations, on Ni-Zn alloys surface compared to pure Ni surface was considered as the primary cause for the decrease of the rate of carbon-carbon formation. Interestingly, another study from the same group revealed that when Ni-Zn alloys was supported on ZnO, resulting from high temperature reduction of Ni/ZnO precursor, the selectivity to ethylene decreased at the benefit to the one to oligomers by comparison with a reference Ni/SiO_2 catalyst [28]. The authors assigned these observations to the negative role of the ZnO support, which favoured the acetylene oligomerization. This is not the case when the Ni-Zn alloys are supported on TiO_2, as the selectivity to oligomers decreases from 38% for Ni down to 5% for NiZn5. It is worth to note that the formation of a green oily liquid was clearly visible in the reactor containing

Ni/TiO_2 when it was removed from the oven at the end of reaction but not in the case of $Ni-Zn/TiO_2$ catalysts, for which only droplets were visible on the walls at the outlet of the reactor. Thermogravimetric analyses reported in Figure 7 were performed under air for the various catalysts after the stability tests (Figure 6). The highest weight loss (15.5%) was observed for the monometallic Ni catalyst. The sequence of weight loss for the bimetallic Ni-Zn catalysts follows the deactivation profiles observed in Figure 6a, that is NiZn5, with the slowest deactivation rate, presents the lowest weight loss (8.2%) whereas NiZn1 and NiZn3 have very close ones (around 10.5%). All the samples show two peaks located around 300 and 390 °C in the differential thermogravimetric profiles (inset in Figure 7), which were previously assigned to heavy hydrocarbons adsorbed on the catalyst surface and to coke on or in the vicinity of Pd, respectively, for Pd/SiO_2 catalysts [59].

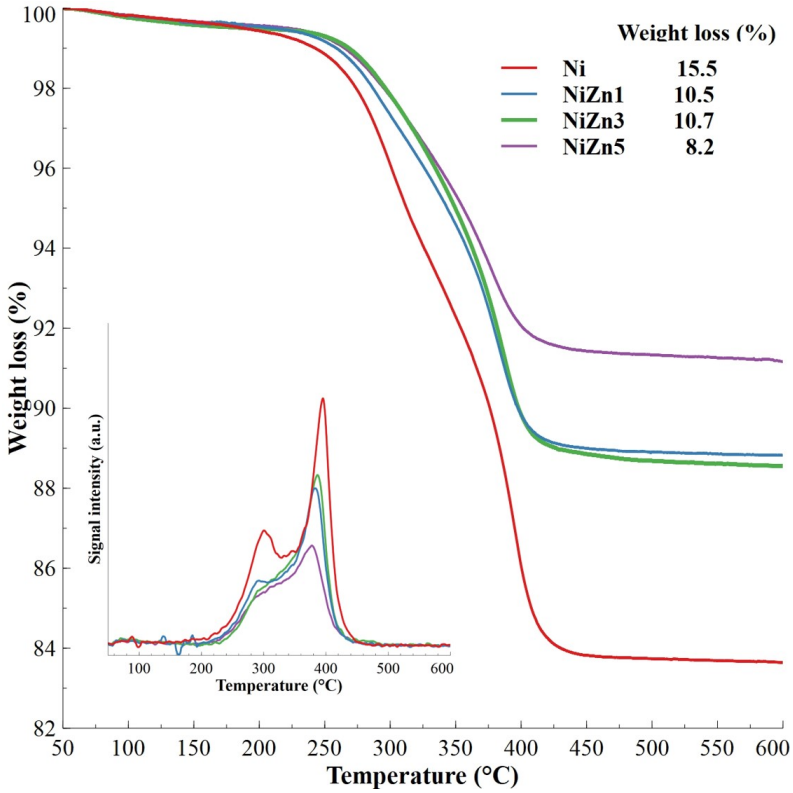

Figure 7. Thermogravimetric analyses performed in air after 20 h of acetylene stability test (Figure 6) for the calcined then reduced Ni and $Ni-Zn/TiO_2$ catalysts. The catalysts were separated from SiC by crushing then sieving. Inset : Differential thermogravimetric analysis for the same samples.

However, the stability of the catalysts is not directly correlated with the selectivity to oligomers. Indeed, Ni/TiO_2 is the most stable catalyst although it presents the highest selectivity to oligomers whereas the bimetallic Ni-Zn samples deactivate gradually with time while forming less oligomers. The effect of polymers formation, such as green oil in acetylene hydrogenation, on the catalyst stability is controversial in the literature. Catalysts deactivation can result from several causes involving various chemical, thermal and mechanical phenomena (i.e., poisoning, fouling, thermal degradation, vapour-solid and solid-solid reactions, and attrition/crushing) [60]. Green oil (paraffin and olefinic hydrocarbons in the C_8–C_{24} range) is often considered as responsible for the deactivation of Pd based selective hydrogenation catalysts by reducing the surface area, blocking the active sites and inhibiting the adsorption and activation of the alkyne and H_2 reactants [61, 62]. However, the extent of the formation of such carbonaceous deposit is not always linked to the loss of activity of the catalysts, as limited deactivation was obtained for Pd based catalysts presenting a content of 36 wt% of carbonaceous deposit [63]. The deactivation of Pd/SiO_2 catalysts in acetylene hydrogenation was shown to occur in three stages [59, 62]. In particular, in a first stage, large amount of relatively light green oil (up to 35 wt%) is formed on the catalyst but acetylene can adsorb on such green oil and then be hydrogenated to ethylene by an hydrogen transfer mechanism. During this stage, the activity of the catalysts only slightly decreases. Moreover, a part of this light and volatile green oil can be hydrogenated and thus removed from the surface, provided that the hydrogen surface concentration is sufficient. As the carbonaceous deposits accumulate on the catalyst surface, polymerization to heavier green oil occurs in a second stage (up to 55 wt%), which can move from the Pd surface to the support. This stage also results in a limited loss of conversion. The major part of the deactivation, in the third stage, was assigned to the blocking of the catalyst pores by the accumulation of green oil, which strongly limits the hydrogen diffusion to the active surface [62]. It is plausible that the same phenomenon occurs in the case of the Ni/TiO_2 catalyst and

that the high H_2/C_2H_2 molar ratio of 10 used in this study favours the hydrogenation of the light green oil formed, limiting its deactivation for this reaction time. Regarding the Ni-Zn/TiO_2 catalysts, the formation of bimetallic Ni-Zn nanoparticles may decrease the surface hydrogen coverage, which makes it more difficult to hydrogenate the light green oil, leading to some early deactivation. However, it is difficult to explain the different deactivation behaviour of the various Ni-Zn/TiO_2 catalysts on the single basis of the Zn content provided by XRF.

The small size of the acetylene molecule and the very strong interaction of the reaction intermediates with transition metal surfaces make its semi-hydrogenation highly challenging in terms of selectivity by comparison with other alkynes or dienes [64]. The supported Ni-Zn bimetallic system appears as a good candidate for this reaction as a rather high selectivity to ethylene can be achieved (above 80%) even at high conversion as predicted in [25]. However, in line with what was previously demonstrated by Spanjers et al [27], the gain in selectivity to ethylene is due to the reduction of the amount of oligomers formed and not to the suppression of the overhydrogenation to ethane.

3.2.2 Hydrogenation of butadiene in an excess of propene

The catalytic performances of the Ni-Zn/TiO_2 samples were also evaluated in the selective hydrogenation of butadiene in the presence of an excess of propene.

Figure 8a shows the evolution of the catalytic activity during temperature programmed reaction between 10 and 80 °C. Zn(2.5 wt%)/TiO_2 does not present any activity in the temperature range 30-150 °C (not shown). As for acetylene hydrogenation, the monometallic Ni/TiO_2 samples is the most active. It presents the lowest full butadiene conversion temperature ($T_{100\%}$), around 35 °C. The introduction of increasing amounts of Zn leads to an increase of the $T_{100\%}$, that is 45 °C for NiZn1 and NiZn3 and 50 °C for NiZn5. The activity ($mol_{butadiene}\ s^{-1}\ g_{Ni}^{-1}$) and turnover frequencies (TOF, s^{-1}) calculated at 20 °C are listed in Table 2 (see

supplementary information for detailed calculations). Among the bimetallic samples, NiZn3 shows the highest catalytic activity (TOF), the two others presenting very similar TOF values to monometallic Ni/TiO_2. Again, the difficulties concerning the precise determination of bimetallic nanoparticles composition make it necessary to take these values cautiously.

For the reaction of semi-hydrogenation of butadiene in the presence of an excess of propene, the catalytic selectivity to alkenes can be considered either from the side of the butenes (1-butene, trans-2-butene and cis-2-butene) formation (Figure 8b) or from the side of the outlet alkanes (butane and propane) concentration (Figure 8c) (see supplementary information for detailed calculations). First, it can be seen from Figure 8-b,c that both monometallic Ni and bimetallic Ni-Zn catalysts have high selectivity to alkenes at temperature lower than $T_{100\%}$. Figure 8b shows that all the catalysts exhibit a progressive decrease of the selectivity to butenes, which coincides with the increase in the selectivity to butane (not shown), as the reaction temperature becomes close to $T_{100\%}$. At butadiene conversion close to 100%, NiZn3 and NiZn5 produce more alkanes than Ni/TiO_2 (this was also the case for acetylene hydrogenation (Figure 5c)), but the concentration of alkanes remains lower than 10%, indicating that all the catalysts are very selective to alkenes (Figure 8c).

The catalytic stability of the samples was compared at similar initial butadiene conversion (80-90%), which also means at different reaction temperatures (20 to 35 °C) (Figure 9a). For the monometallic Ni catalyst, the butadiene conversion decreases to below 10% during the first 10 h of reaction at 20 °C. After an initial loss of activity in the first hours of reaction, the bimetallic Ni-Zn/TiO_2 catalysts, especially the NiZn5 sample, present only limited deactivation at 25 °C and 35 °C.

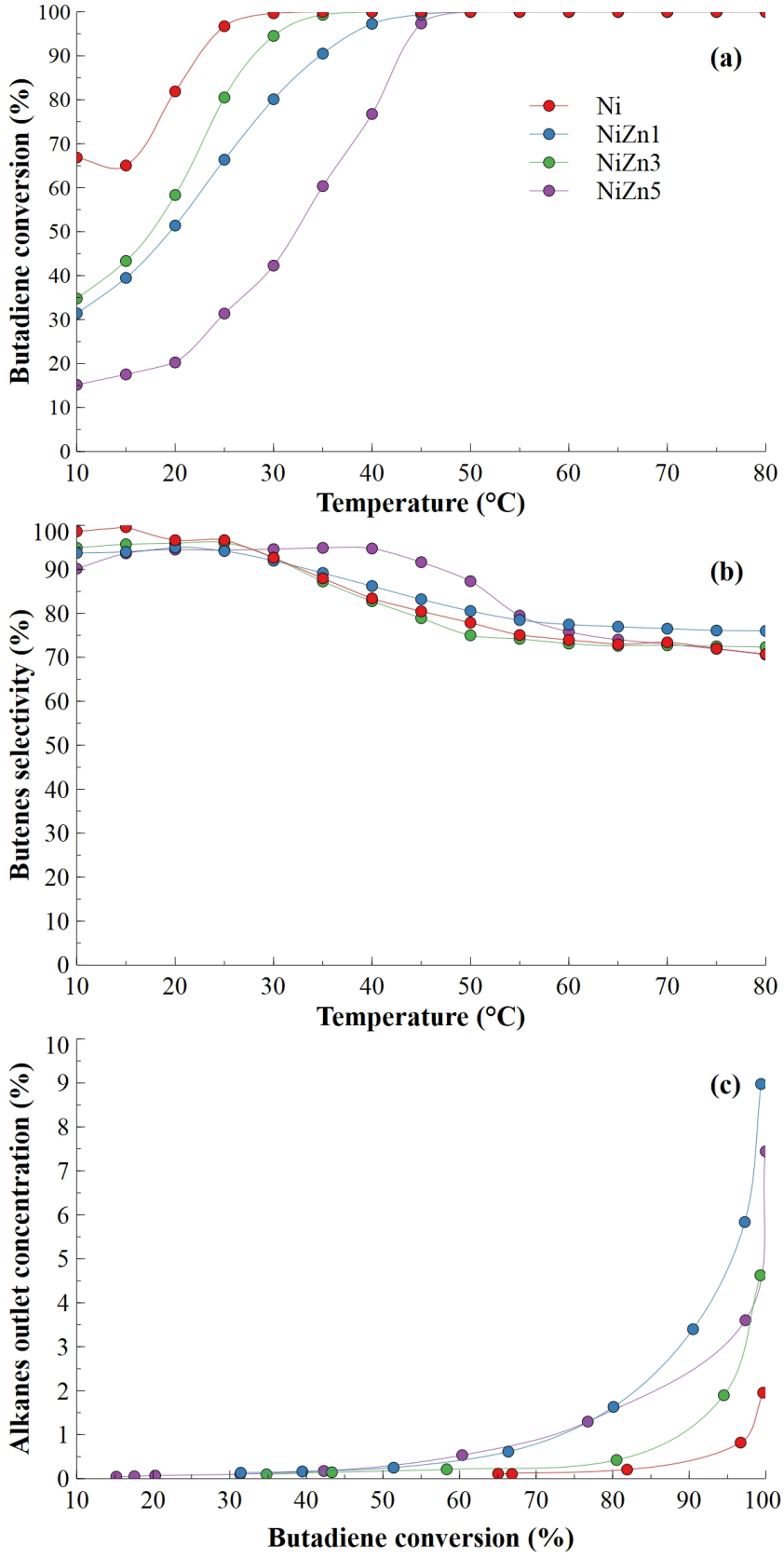

Figure 8. Evolution with reaction temperature of the butadiene conversion (a), the selectivity to butenes (1-butene + cis-2-butene + trans-2-butene) (b) and outlet alkanes concentration as a function of butadiene conversion (c) for the calcined then reduced Ni and Ni-Zn/TiO_2 catalysts (0.5 wt% Ni) (10 mg of catalyst diluted with 90 mg TiO_2).

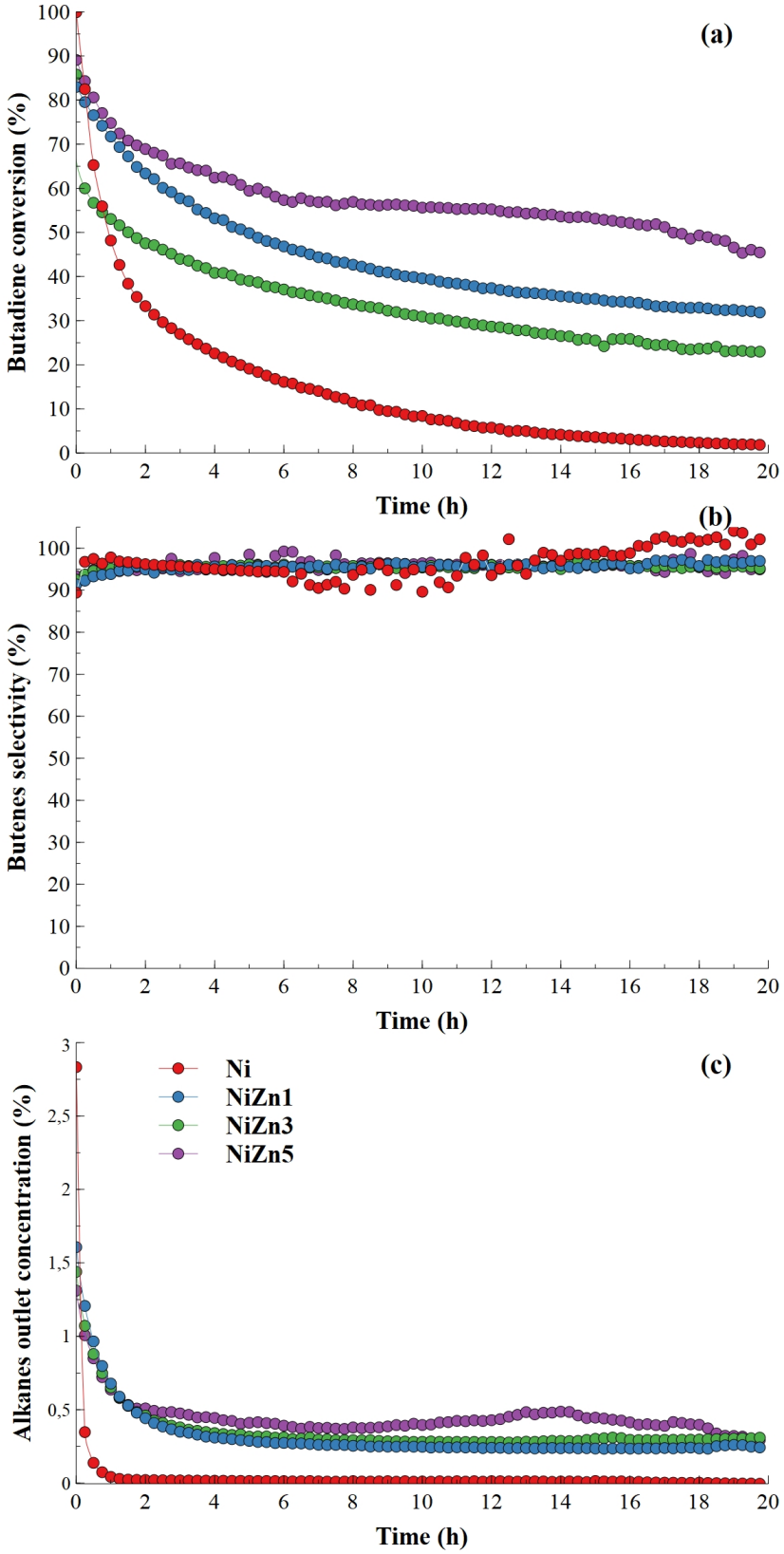

Figure 9. Evolution of the butadiene conversion (a), the selectivity to butenes (b) and the outlet alkanes concentration (c) with time on stream from an initial conversion of about 80-90% (at 20 °C for Ni, 25 °C for NiZn1 and NiZn3, 35 °C for NiZn5) (0.5 wt% Ni) (10 mg of catalyst diluted with 90 mg TiO_2)

In contrast to what was observed during the temperature programmed reaction (Figure 8), the selectivity to butenes remains high (around 95%) for all the catalysts (Figure 9b). The alkanes concentration is below 0.5-1% for all the catalysts and even extremely low for Ni/TiO_2 (Figure 9c), which is probably related to its very pronounced deactivation. The evolution of the selectivities in the various C_4 products (1-butene, cis- and trans-2-butene, butane) with time on stream (Figure S4) reveals that 1-butene is the major product whatever the catalyst and that the proportion of the various butenes remains constant throughout the reaction. The butenes distribution is virtually identical regardless of the Ni/Zn ratio (Figure S4). In the case of selective hydrogenation of polyunsaturated compounds, the formation of carbonaceous foulant is regarded as an important factor of deactivation, as previously discussed for the acetylene hydrogenation reaction, blocking the access to the active sites at the surface of the catalyst [65]. Note that contrary to the incomplete C_2 carbon balance observed for the latter reaction and related to the oligomers formation, the C_4 carbon balance for the butadiene hydrogenation is 97-99% for all the catalysts, indicating that only a marginal part of the C_4 reactant or products could be responsible for the formation of carbonaceous deposit. Regarding the C_3 compounds (propane and propene), the high propene content in the feed (30%) makes the determination of the propene concentration inaccurate and prevents estimating the contribution of propene in the deactivation phenomenon. The temperature of decomposition and the amount of carbonaceous deposited on the catalysts surface after stability test were quantified by thermogravimetric analysis (TGA) performed under air flow (Figure S5). Considering the fact that the catalyst-TiO_2 mixtures used for the stability tests (Figure 9) contained very small amount of Ni (only 0.05 mg of Ni in 100 mg of catalyst/TiO_2 mixture), undiluted Ni/TiO_2 and $Ni\text{-}Zn/TiO_2$ samples were submitted to a stability test at 25 °C for 20 h to better observe the variations of weight loss (Figure S5). A reference analysis was also performed on the bare TiO_2 support, which was calcined then reduced at 450 °C for 2 h, and exposed to the reactant gas mixture at 25 °C for 20

h. In Figure S5, a decrease in the weight of the TiO_2 support (1.2 wt%), can be observed in the temperature range between 150 and 600 °C. It can be assigned to the removal of butadiene/propene adsorbed on the support as it is not active for the reaction. Regarding the Ni containing catalysts, the weight losses in the monometallic Ni and bimetallic Ni-Zn catalysts appear similar and rather close to the one of TiO_2 (Figure S5).

Contrary to what was observed for the acetylene hydrogenation reaction, the addition of Zn to Ni/TiO_2 appears to have a beneficial effect on the stability of the catalysts in butadiene selective hydrogenation. Such a discrepancy might be related either to the difference in concentration of the polyunsaturated reactant in both reaction (2% for acetylene and 0.3% for butadiene) or to the strong tendency of acetylene to undergo coupling reactions, leading to the formation of a high proportion of oligomers (green oil), which is not the case of butadiene in our reaction conditions, as indicated by the C_4 carbon balance. It is possible that the deactivation observed in the case of butadiene hydrogenation is due to the deposition of carbonaceous (coke) species resulting from the interaction of the surface with the various hydrocarbons (alkenes and alkanes) instead of oligomers, which may be favoured by the low reaction temperatures employed (15-35 °C). For Ni-based steam methane reforming (SMR) catalysts (such as $Ni/MgAl_2O_4$), coke formation is considered to originate primarily from alkene formation [60]. A positive effect of Zn addition to Ni catalysts stability has been previously observed for ethanol steam reforming, and it also resulted in a decrease in the formation of carbonaceous deposit [66]. The enhanced stability was ascribed to the formation of Ni-Zn alloy, resulting in the dilution of large surface ensembles of Ni metal atoms by Zn atoms and the according inhibition of carbon deposition [66]. A lower formation of carbonaceous compounds was also observed on a Zn modified Ni/Al_2O_3 catalysts during selective hydrogenation of acetylene [67], however, the authors ascribed this phenomenon to a higher Ni phase dispersion in the zinc aluminate phase formed in ternary Ni-Zn-Al catalyst, and to a decrease in the number of surface

acid sites compared to Ni/Al_2O_3, rather than to the formation of an intermetallic NiZn phase. Although the EDS results (Figure 4) may be questionable due to the possible evaporation of Zn under the beam, they could indicate that a part of Zn is not alloyed with Ni and is present on the TiO_2 surface. Acidic sites are known to promote the adsorption of hydrocarbons and to provoke not only isomerization but also transformation into coke or C_2-C_6 hydrocarbons from cracking and disproportionation reactions [60, 68]. A lower formation of coke on Pd/Zn-modified α-Al_2O_3 was deduced by TGA after acetylene hydrogenation by comparison with the unmodified sample and was assigned to a decrease in the acidity of the surface induced by the Zn addition [69]. However, as previously mentioned, the weight losses observed for all the catalysts by TGA are rather low and similar (Figure S5), which seems to indicate that the carbonaceous deposit during butadiene reaction is limited and could hardly explain the strong deactivation of the Ni/TiO_2 catalyst, all the more so when compared with what has been observed for the hydrogenation of acetylene. Another assumption would be to consider a deactivation caused by the progressive passivation of the Ni nanoparticles surface by traces of O_2 or H_2O present in the reactant feed. Despite the reducing character of the reaction mixture employed, with 20% H_2, the low reaction temperature used for butadiene hydrogenation (20°C for Ni/TiO_2 up to 35°C for $Ni\text{-}Zn/TiO_2$) might not be sufficient to prevent such a surface oxidation. This phenomenon was observed for Ni/Al_2O_3 catalyst in CO_2 methanation, with technical CO_2 containing O_2 impurities and resulted also in a deactivation of the catalyst [70]. A gradual deactivation of the intermetallic compound $Al_{13}Fe_4$ was observed during butadiene hydrogenation in batch reactor and ascribed to surface oxidation by traces of O-containing gas impurities (O_2, H_2O) present in the reactor [71]. In order to explore this hypothesis, a deactivated Ni/TiO_2 catalyst during 5-hour reaction at 20 °C was treated under H_2 at moderate temperature (200 °C) for 1h to estimate whether the deactivation is reversible (Figure S6). From the TGA analyses reported in Figures 7 and S5 and the literature data [60, 72], the removal of

carbonaceous deposit is not expected to occur at such a low temperature. After the treatment under H_2 at 200 °C, the monometallic nickel catalyst resubmitted to the reaction at 20 °C, started again from a high initial butadiene conversion (99%) before gradually deactivating with time in a similar way as in the first run (Figure S6). A second H_2 treatment led to the same recovery of the high initial conversion followed by a similar period of deactivation (Figure S6). As a comparison, the NiZn5 catalyst tested under the same conditions, which was much more stable, and showed only very moderate deactivation in the 5h reaction time, also restored its high initial conversion after treatment under H_2. It appears from this experiment that Ni/TiO_2 can be regenerated by a reduction treatment in mild conditions, which support the assumption of a deactivation by surface oxidation of the Ni nanoparticles. The formation of bimetallic Ni-Zn particles in the Ni-Zn/TiO_2 samples may prevent or at least slow down the oxidation of Ni, as previously reported for Urushibara Nickel catalysts (analogous to Raney Nickel) in which the presence of metallic Zn protects the nickel from oxidation in mild oxidative conditions [73]. Similarly, Mg-Al mixed oxide supported Ni-Zn catalyst showed enhanced resistance against Ni re-oxidation in methane tri-reforming at 800 °C and the protective effect of Zn was ascribed to the strong oxophilic character of Zn, which prevents the oxidation of Ni [74]. This stabilization of the active metallic Ni sites by the presence of Zn could thus account for the higher stability of the Ni-Zn/TiO_2 catalysts in butadiene hydrogenation. In the case of acetylene hydrogenation, the higher temperature of reaction (165-175 °C) may limit this possible oxidation in reducing atmosphere, resulting in a more stable Ni catalyst.

3. CONCLUSION

In this contribution, TiO_2-supported bimetallic Ni-Zn catalysts prepared by co-deposition-precipitation with urea, with low Ni loadings (0.5 wt%), demonstrated relatively high selectivity to alkenes (85% to ethylene and 95% to butenes) with very limited alkanes formation in the reactions of selective hydrogenation of pure acetylene and of butadiene in the presence of an excess of propene, respectively. One of the main effects of the combination of Ni with Zn is to reduce the formation of oligomers in acetylene hydrogenation, underlining again that a low production of ethane is not the only parameter to identify a selective catalyst in this type of reaction.

Whilst the Ni-Zn samples could maintain a good level of conversion during around 20h time on stream (from 80-90% to around 60%) for butadiene selective hydrogenation at low temperature ($\leq$ 35 °C) whereas monometallic Ni deactivated rapidly, a reverse trend was observed for acetylene hydrogenation performed at higher temperature (> 165 °C). It shows that, although these two reactions can be classified as analogous, the behavior of the catalysts strongly depends on the structure of the polyunsaturated hydrocarbon and/or the reaction conditions. Improving the stability of these catalysts is therefore an important step to consider their use as an alternative to standard commercial PdAg catalysts. The main limitation encountered in this study is the difficulty to control the composition of the bimetallic NiZn nanoparticles after reduction under H_2 due to the proximity of the Ni^{2+} reduction and Zn sublimation temperatures. Among the paths envisaged to improve the performance of these NiZn catalysts, the development of synthesis methods allowing a finer control of their composition can be considered as a judicious approach.

ACKNOWLEDGMENT

Dr. Zhao Wang thanks the China Scholarship Council (CSC) for his PhD scholarship. The authors thank the French METSA network for free access to JEOL ARM 200F microscope. Zhao Wang also thanks Prof. Haolin Tang, and Prof. Haining Zhang for their suggestions on writing manuscript.

REFERENCES

1. B.J. Burger, M.E. Thompson, W.D. Cotter, J.E. Bercaw, J. Am. Chem. Soc. **112**, 1566 (1990)
2. N.S. Schbib, M.A. García, C.E. Gígola, A.F. Errazu, Ind. Eng. Chem. Res. **35**, 1496 (1996)
3. E.L. Mohundro, in American Institute of Chemical Engineers 15th Ethylene Producers Conference, New Orleans(2003)
4. M.L. Derrien, in Studies in Surface Science and Catalysis, ed. L. Cerveny (Elsevier, 1986), pp. 613-666
5. F.H. Puls, K.D. Ruhnke, (United States Exxon Research & Engineering Co. (Florham Park, NJ) 4260840 1981)
6. J. Howeizi, S. Taghvaei-Ganjali, M. Malekzadeh, F. Motiee, S. Sahebdelfar, Res. Chem. Intermed. **45**, 3165 (2019)
7. R.J. Gartside, T. Skourlis, (Lummus Technology Inc. (1515 Broad Street, Bloomfield NJ 07003-3096, US) EP1773739, 2007)
8. S.A. Blankenship, R.W. Voight, J.A. Perkins, J.E. Fried Jr, (Google Patents, 2003)
9. Q. Zhang, J. Li, X. Liu, Q. Zhu, Appl. Catal., A **197**, 221 (2000)
10. W. Ludwig, A. Savara, R.J. Madix, S. Schauermann, H.-J. Freund, J. Phys. Chem. C **116**, 3539 (2012)
11. W. Ludwig, A. Savara, K.-H. Dostert, S. Schauermann, J. Catal. **284**, 148 (2011)
12. M. Wilde, K. Fukutani, W. Ludwig, B. Brandt, J.H. Fischer, S. Schauermann, H.J. Freund, Angew. Chem. Int. Ed. **47**, 9289 (2008)
13. B. Ngamsom, N. Bogdanchikova, M.A. Borja, P. Praserthdam, Catal. Commun. **5**, 243 (2004)
14. A. Pachulski, R. Schödel, P. Claus, Appl. Catal., A **400**, 14 (2011)
15. S. Komeili, M.T. Ravanchi, A. Taeb, Res. Chem. Intermed. **44**, 1335 (2018)
16. M.T. Ravanchi, S. Fadaeerayeni, M.R. Fard, Res. Chem. Intermed. **42**, 4797 (2016)
17. D. Teschner, J. Borsodi, A. Wootsch, Z. Révay, M. Hävecker, A. Knop-Gericke, S.D. Jackson, R. Schlögl, Science **320**, 86 (2008)
18. N.A. Khan, S. Shaikhutdinov, H.-J. Freund, Catal. Lett. **108**, 159 (2006)
19. G. Vilé, D. Albani, N. Almora-Barrios, N. López, J. Pérez-Ramírez, ChemCatChem **8**, 21 (2016)
20. C. Louis, L. Delannoy, in Advances in Catalysis, Vol 64, ed. C. Song (2019), pp. 1-88
21. L.L. Zhang, M.X. Zhou, A.Q. Wang, T. Zhang, Chem. Rev. **120**, 683 (2020)
22. R. Hou, W. Yu, M.D. Porosoff, J.G. Chen, T. Wang, J. Catal. **316**, 1 (2014)
23. S. Leviness, V. Nair, A.H. Weiss, Z. Schay, L. Guczi, J. Mol. Catal. **25**, 131 (1984)
24. P.T. Witte, P.H. Berben, S. Boland, E.H. Boymans, D. Vogt, J.W. Geus, J.G. Donkervoort, Top. Catal. **55**, 505 (2012)
25. F. Studt, F. Abild-Pedersen, T. Bligaard, R.Z. Sørensen, C.H. Christensen, J.K. Nørskov, Science **320**, 1320 (2008)
26. Z. Wang, G. Wang, C. Louis, L. Delannoy, J. Catal. **347**, 185 (2017)
27. C.S. Spanjers, J.T. Held, M.J. Jones, D.D. Stanley, R.S. Sim, M.J. Janik, R.M. Rioux, J. Catal. **316**, 164 (2014)
28. C.S. Spanjers, R.S. Sim, N.P. Sturgis, B. Kabius, R.M. Rioux, ACS Catal. **5**, 3304 (2015)
29. M. Kang, M.W. Song, T.W. Kim, K.L. Kim, Can. J. Chem. Eng. **80**, 63 (2002)
30. B. Bridier, N. López, J. Pérez-Ramírez, Dalton Trans. **39**, 8412 (2010)
31. H. Li, H. Li, W.-L. Dai, W. Wang, Z. Fang, J.-F. Deng, Appl. Surf. Sci. **152**, 25 (1999)
32. S.P. Lee, Y.W. Chen, J. Chem. Technol. Biotechnol. **75**, 1073 (2000)

33. S. Yoshida, H. Yamashita, T. Funabiki, T. Yonezawa, J. Chem. Soc., Faraday Trans. 1 F **80**, 1435 (1984)
34. Y. Liu, X. Liu, Q. Feng, D. He, L. Zhang, C. Lian, R. Shen, G. Zhao, Y. Ji, D. Wang, Adv. Mater. **28**, 4747 (2016)
35. Y. Chen, J. Chen, Appl. Surf. Sci. **387**, 16 (2016)
36. K. Bourikas, C. Kordulis, A. Lycourghiotis, Chem. Rev. **114**, 9754 (2014)
37. P. Burattin, M. Che, C. Louis, J. Phys. Chem. B **102**, 2722 (1998)
38. A. Aguilar-Tapia, L. Delannoy, C. Louis, C.W. Han, V. Ortalan, R. Zanella, J. Catal. **344**, 515 (2016)
39. G. Yuan, C. Louis, L. Delannoy, M.A. Keane, J. Catal. **247**, 256 (2007)
40. D.M. Fernandes, R. Silva, A.A.W. Hechenleitner, E. Radovanovic, M.A.C. Melo, E.A.G. Pineda, Mater. Chem. Phys. **115**, 110 (2009)
41. C. Ricolleau, J. Nelayah, T. Oikawa, Y. Kohno, N. Braidy, G. Wang, F. Hue, L. Florea, V. Pierron Bohnes, D. Alloyeau, Microscopy **62**, 283 (2013)
42. A. Hugon, L. Delannoy, J.-M. Krafft, C. Louis, J. Phys. Chem. C **114**, 10823 (2010)
43. T. Imoto, Y. Harano, Y. Nishi, S. Masuda, Bull. Chem. Soc. Jpn. **37**, 441 (1964)
44. S. Lew, A.F. Sarofim, M. Flytzani-Stephanopoulos, Chem. Eng. Sci. **47**, 1421 (1992)
45. M. Liang, W. Kang, K. Xie, J. Nat. Gas Chem. **18**, 110 (2009)
46. M.A. Valenzuela, P. Bosch, J. Jiménez-Becerrill, O. Quiroz, A.I. Páez, J. Photochem. Photobiol., A **148**, 177 (2002)
47. K. Hadjiivanov, M. Mihaylov, N. Abadjieva, D. Klissurski, J. Chem. Soc., Faraday Trans. **94**, 3711 (1998)
48. J. van de Loosdrecht, A.M. van der Kraan, A.J. van Dillen, J.W. Geus, J. Catal. **170**, 217 (1997)
49. D. Kohl, M. Henzler, G. Heiland, Surf. Sci. **41**, 403 (1974)
50. D.F. Anthrop, A.W. Searcy, J. Phys. Chem. **68**, 2335 (1964)
51. W. Pearson, W. Pearson, An Alphabetical Index of Work on Metals and Alloys, 1958)
52. I.S. Mashkovsky, G.N. Baeva, A.Y. Stakheev, M.N. Vargaftik, N.Y. Kozitsyna, Moiseev, II, Mendeleev Commun. **24**, 355 (2014)
53. D.L. Trimm, N.W. Cant, I.O. Liu, Catal. Today **178**, 181 (2011)
54. B. Hammer, J.K. Nørskov, Adv. Catal. **45**, 71 (2000)
55. G. Bond, Discuss. Faraday Soc. **41**, 200 (1966)
56. A.H. Al-ShaikhAli, A. Jedidi, L. Cavallo, K. Takanabe, Chem. Commun. **51**, 12931 (2015)
57. A.H. Al-ShaikhAli, A. Jedidi, D.H. Anjum, L. Cavallo, K. Takanabe, ACS Catal. **7**, 1592 (2017)
58. R.T. Vang, K. Honkala, S. Dahl, E.K. Vestergaard, J. Schnadt, E. Lægsgaard, B.S. Clausen, J.K. Nørskov, F. Besenbacher, Nat. Mater. **4**, 160 (2005)
59. W.-J. Kim, S.H. Moon, Catal. Today **185**, 2 (2012)
60. M.D. Argyle, C.H. Bartholomew, Catalysts **5**, 145 (2015)
61. M.T. Ravanchi, S. Sahebdelfar, S. Komeili, Rev. Chem. Eng. **34**, 215 (2018)
62. I.Y. Ahn, J.H. Lee, S.K. Kim, S.H. Moon, Appl. Catal., A **360**, 38 (2009)
63. A. Sárkány, L. Guczi, A.H. Weiss, Appl. Catal. **10**, 369 (1984)
64. Á. Molnár, A. Sárkány, M. Varga, J. Mol. Catal. A: Chem. **173**, 185 (2001)
65. M. Stammbach, D. Thomas, D. Trimm, M. Wainwright, Appl. Catal. **58**, 209 (1990)
66. C. Anjaneyulu, L.O. da Costa, M.C. Ribeiro, R.C. Rabelo-Neto, L.V. Mattos, A. Venugopal, F.B. Noronha, Appl. Catal., A **519**, 85 (2016)
67. J. Rodrıguez, A. Marchi, A. Borgna, A. Monzón, J. Catal. **171**, 268 (1997)
68. P. Berteau, S. Ceckiewicz, B. Delmon, Appl. Catal. **31**, 361 (1987)

69. S. Chinayon, O. Mekasuwandumrong, P. Praserthdam, J. Panpranot, Catal. Comm. **9**, 2297 (2008)
70. B. Mutz, A.M. Ganzler, M. Nachtegaal, O. Muller, R. Frahm, W. Kleist, J.D. Grunwaldt, Catalysts **7**, 279 (2017)
71. L. Piccolo, L. Kibis, J. Catal. **332**, 112 (2015)
72. J.L. Figueiredo, (Springer Netherlands, Dordrecht, 1982), pp. 45-63
73. I. Jacob, M. Fisher, Z. Hadari, M. Herskowitz, J. Wlsniak, N. Shamir, M.H. Mintz, J. Catal. **101**, 28 (1986)
74. R. Kumar, K.K. Pant, Appl. Surf. Sci. **515**, 146010 (2020)

First memories of Michel Che

Michel Che was already the head of the LRS lab, when in 1979, I (Catherine Louis) chose to do my PhD under his direction. He had been appointed as a full Professor, a few years before, (coming from the Institut de Catalyse in Lyon where his main research focused on the characterization of oxide defects and oxide doping by EPR). His first research fields at LRS concerned the study of the physico-chemical phenomena occurring during the preparation of supported catalysts in order to better control the dispersion of the supported phase. When I arrived, the lab did not have many characterisation techniques. I remember an old EPR spectrometer in one room and in the preparation room, of two glass vacuum lines with mercury pumps and grease stopcocks, in which the catalysts were pretreated under different gas before EPR characterisation. There were also UV-Visible and IR spectrometers. During the 5 years of my PhD, I directly worked under his supervision to develop a method of preparation allowing to disperse Mo ions as better as possible on a silica support. The EPR spectroscopy was my main technique to characterize the Mo dispersion (in fact Mo^{5+}) and to study various reactions of electron transfer at the surface of Mo/SiO_2.
I remember the one-on-one scientific meetings with him and his long monologues from which I had afterwards to extract the follow-up to be given to my work, which was a way to let me free to direct my research on my own.
Under his direction, the LRS laboratory has gradually grown, equipping itself with numerous state-of-the-art characterization devices, recruiting many researchers and lecturers over the years, and gradually gaining national and international recognition.

Supplementary Information

Bimetallic Ni-Zn/TiO_2 catalysts for selective hydrogenation of alkyne and alkadiene impurities from alkenes stream

Zhao Wang[1,3], Guillaume Wang[2], Catherine Louis[1], Laurent Delannoy[1*]

1- Sorbonne Université, CNRS, Laboratoire de Réactivité de Surface, LRS, F-75252 Paris, France.

2- Université Paris Diderot, Sorbonne Paris Cité, CNRS, Laboratoire Matériaux et Phénomènes Quantiques, UMR 7162, 75013, Paris, France.

3-Present address: State Key Laboratory Advance Technology for Materials Synthesis and Processing, School of Materials Science and Engineering, Wuhan University of Technology, 122, Luoshi Road, Wuhan, 430070, China.

Catalytic performances evaluation

Gases. The gases used for the catalyst preparation and testing were purchased from Air Liquide France: Propylene 3.5 (99.5% purity), 1,3-butadiene (6000 ppm mixture in He), H_2 (99.999% purity), Helium (99.999% purity), Synthetic Air (99.99% purity) and N_2 (99.999% purity).

Conversion and selectivities

1) **Hydrogenation of Acetylene :**

$$\text{Conversion}_{\text{Acetylene}} = \frac{\text{Acetylene}_{\text{in}} - \text{Acetylene}_{\text{out}}}{\text{Acetylene}_{\text{in}}}$$

$$\text{Selectivity}_{\text{Ethylene}} = \frac{\text{Ethylene}_{\text{out}}}{\text{Acetylene}_{\text{in}} - \text{Acetylene}_{\text{out}}}$$

$$\text{Selectivity}_{\text{Ethane}} = \frac{\text{Ethane}_{\text{out}}}{\text{Acetylene}_{\text{in}} - \text{Acetylene}_{\text{out}}}$$

$$\text{Selectivity}_{\text{oligomers}} = 1 - (\text{Selectivity}_{\text{Ethylene}} + \text{Selectivity}_{\text{Ethane}})$$

2) **Selective hydrogenation of butadiene in excess of propene :**

$$\text{Conversion}_{\text{Butadiene}} = \frac{\text{Butadiene}_{\text{in}} - \text{Butadiene}_{\text{out}}}{\text{Butadiene}_{\text{in}}}$$

$$\text{Selectivity}_{\text{butenes}} = \frac{\sum \text{Butenes}_{\text{out}}}{\text{Butadiene}_{\text{in}} - \text{Butadiene}_{\text{out}}}$$

$$\text{with } \sum \text{Butenes}_{\text{out}} = \text{1\_butene}_{\text{out}} + \text{cis\_2\_butene}_{\text{out}} + \text{trans\_2\_butene}_{\text{out}}$$

$$\text{Alkanes concentration} = \frac{\text{Propane}_{\text{out}} + \text{Butane}_{\text{out}}}{\text{Propane}_{\text{out}} + \text{Butane}_{\text{out}} + \sum \text{Butenes}_{\text{out}} + \text{Butadiene}_{\text{out}} + \text{Propene}_{\text{in}}}$$

Activity and turnover frequency (TOF)

The catalytic activity is expressed considering that Ni is the only active metal for the reaction and as follows:

$$\text{Activity}\ (\text{mol}\cdot\text{s}^{-1}\cdot\text{g}_{\text{Ni}}^{-1}) = \frac{\text{Reactant conversion}\times Q_{\text{reactant}}}{m_{\text{catalyst}}\times \text{wt\%Ni}} \qquad (1)$$

Reactant conversion is the conversion of acetylene or butadiene; $Q_{reactant}$ is the molar flow rate ($mol.s^{-1}$) of the reactant (acetylene or butadiene) at room temperature, $m_{catalyst}$ is the catalyst mass used for the test, wt% Ni is the Ni loading of the catalyst determined by XRF;

$$\text{TOF}(s^{-1}) = \frac{\text{Activity}\cdot M_{\text{Ni}}}{\text{Dispersion}} \qquad (2)$$

Dispersion is the metal dispersion, which was calculated from equation (3) using the formula described by Scholten [1]:

$$D = 10^{21} \times \frac{6 \times M \times \rho_{site}}{d \times \rho_{metal} \times N} \qquad (3)$$

for which M is the metal atomic weight ($g\ mol^{-1}$); ρ_{site} is the metal surface site density; d is the average particle size; ρ_{metal} is the metal density (8.908 $g\ cm^{-3}$ for nickel); N is the Avogadro constant ($6.02\times10^{23}\ mol^{-1}$). For monometallic nickel, $\rho_{site\ Ni}$ is equal to 15.4 atoms nm^{-2} according to [1]. For the NiZn catalysts, the surface metal density ($\rho_{site\ NiZn}$) was estimated using the average Ni/Zn atomic ratios deduced from the XRF measurements obtained for each Ni-Zn/TiO_2 samples after reduction by the relation

$$\rho_{\text{site NiZn}} = \rho_{\text{site Ni}} \times \frac{\frac{\text{Ni}}{\text{Zn}}}{1+\frac{\text{Ni}}{\text{Zn}}}$$

In this calculation, it is also assumed that the surface composition of the particles is the same as the bulk composition.

Reference

1. J. Scholten, A. Pijpers, A. Hustings, Catal. Rev. 27, 151 (1985)

Figure S1: XRD of calcined then reduced DPU NiZn 1:5/TiO_2 sample.

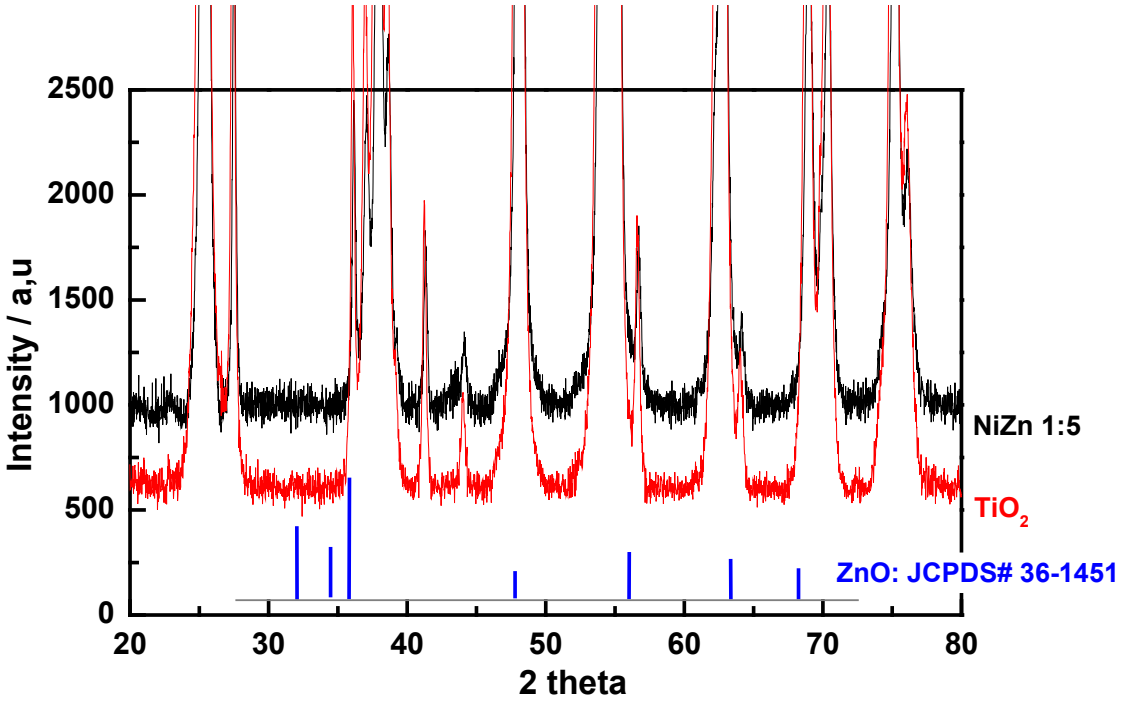

Table S1: Percentage of reduced Ni^{2+} calculated from the TPR

	Sample	Sample weight for TPR / mg	NiO weight / mg	Integrated area from TPR data	Maximum of reduction peak in TPR / ^{o}C	Reduced NiO calculated from TPR / mg	Percentage of reduced Ni^{2+} (%)
Reference	**NiO**	**112.5**	**112.5**	**647**	**430**	**112.5**	**100**
Catalysts	**Ni**	**113.5**	**0.780**	**3.72**	**400**	**0.65**	**83**
	NiZn1	**114.5**	**0.720**	**3.91**	**410**	**0.68**	**94**
	NiZn3	**110.6**	**0.700**	**4.48**	**430**	**0.78**	**111**
	NiZn5	**101.1**	**0.710**	**3.94**	**440**	**0.69**	**97**

Figure S2: Evolution of the selectivity to oligomers with acetylene conversion during temperature programmed reaction of acetylene hydrogenation for the calcined then reduced Ni and Ni-Zn/TiO_2 catalysts (0.5 wt% Ni) (50 mg of catalyst diluted with 150 mg SiC).

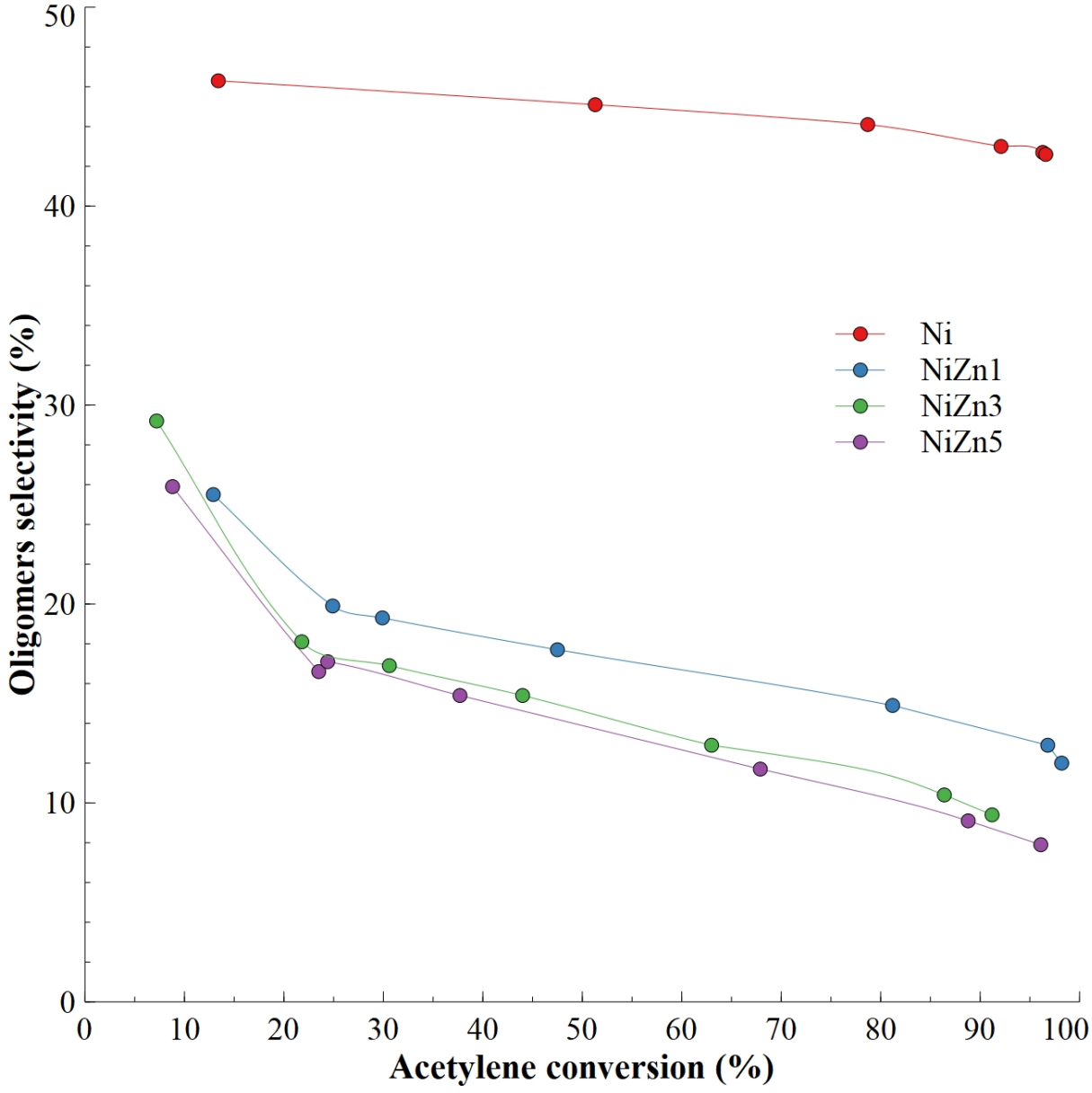

Figure S3: Evolution of the selectivity to ethane (a) and oligomers (b) with time on stream during acetylene hydrogenation for the calcined then reduced Ni and Ni-Zn/TiO_2 catalysts (0.5 wt% Ni) (50 mg of catalyst diluted with 150 mg SiC).

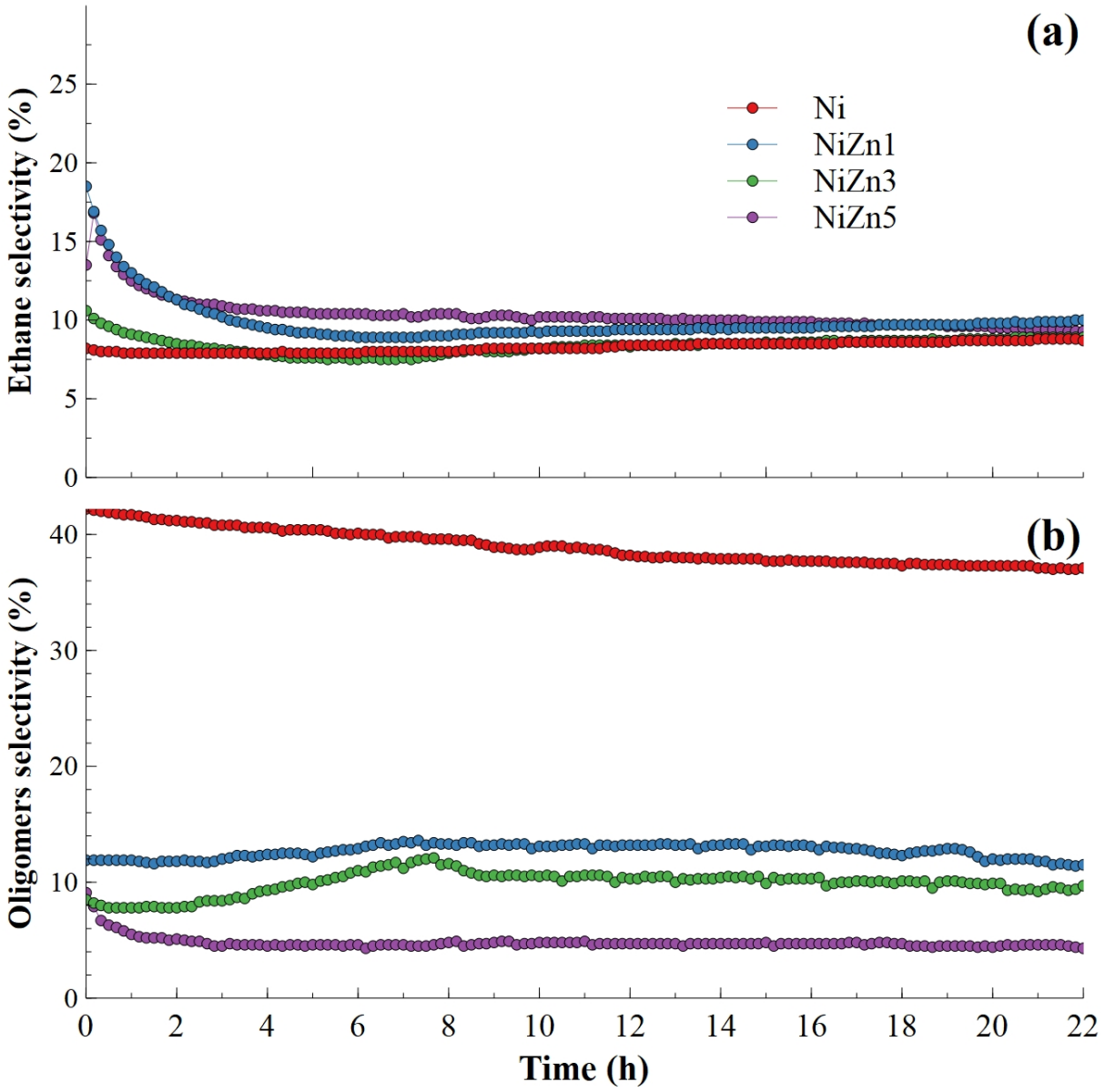

Figure S4: Evolution of the selectivity to 1-butene, trans-2-butene, cis-2-butene and butane with time on stream during butadiene hydrogenation for the calcined then reduced Ni and Ni-Zn/TiO_2 catalysts (0.5 wt% Ni) (10 mg of catalyst diluted with 90 mg TiO_2).

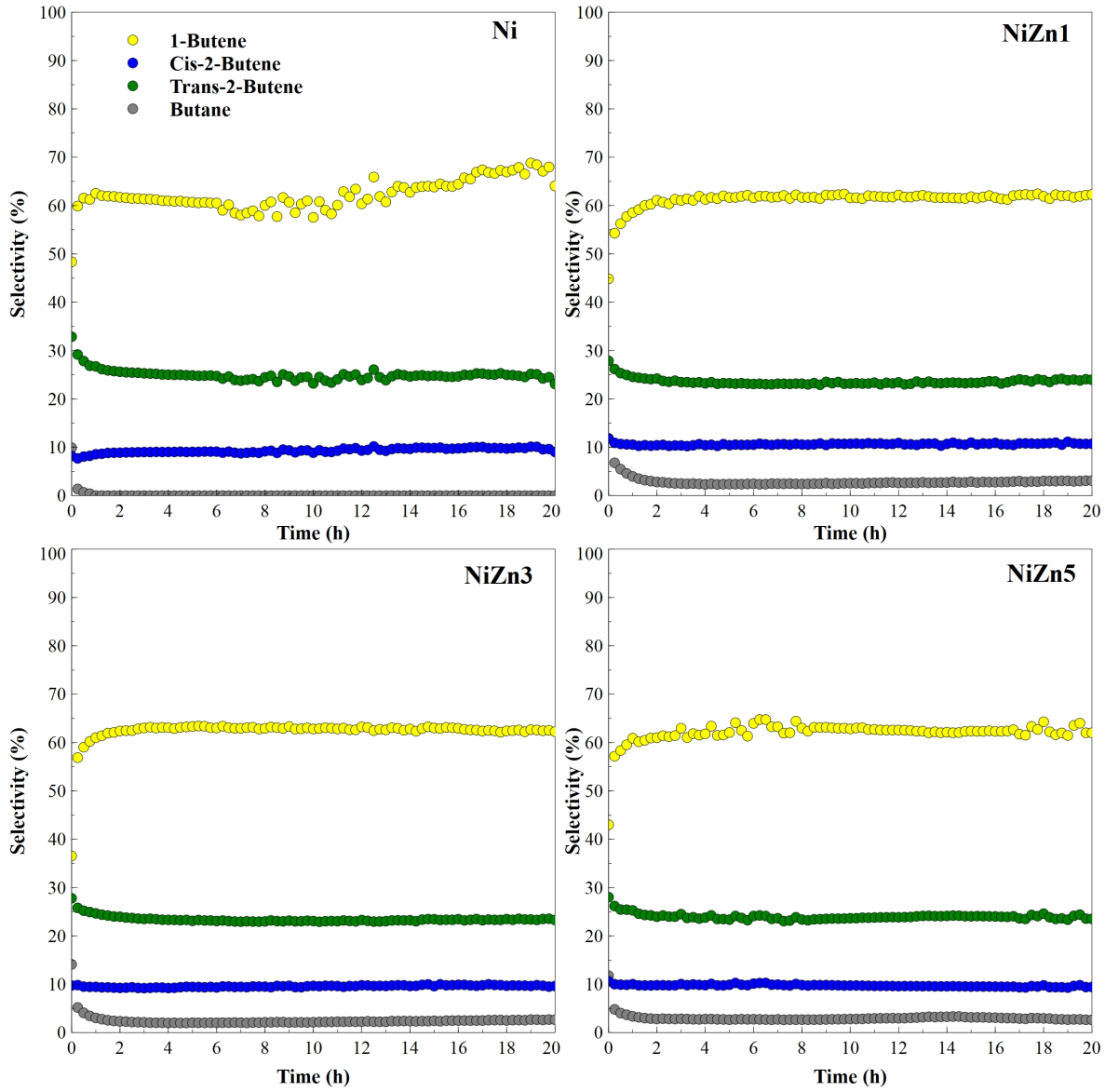

Figure S5: Thermogravimetric analyses performed in air of TiO_2 support and undiluted Ni-Zn/TiO_2 samples after 20 h of butadiene hydrogenation test at 25 °C. TiO_2 was previously calcined then reduced at 450 ºC and exposed to reactant gas mixture for 20 h at 25 ºC.

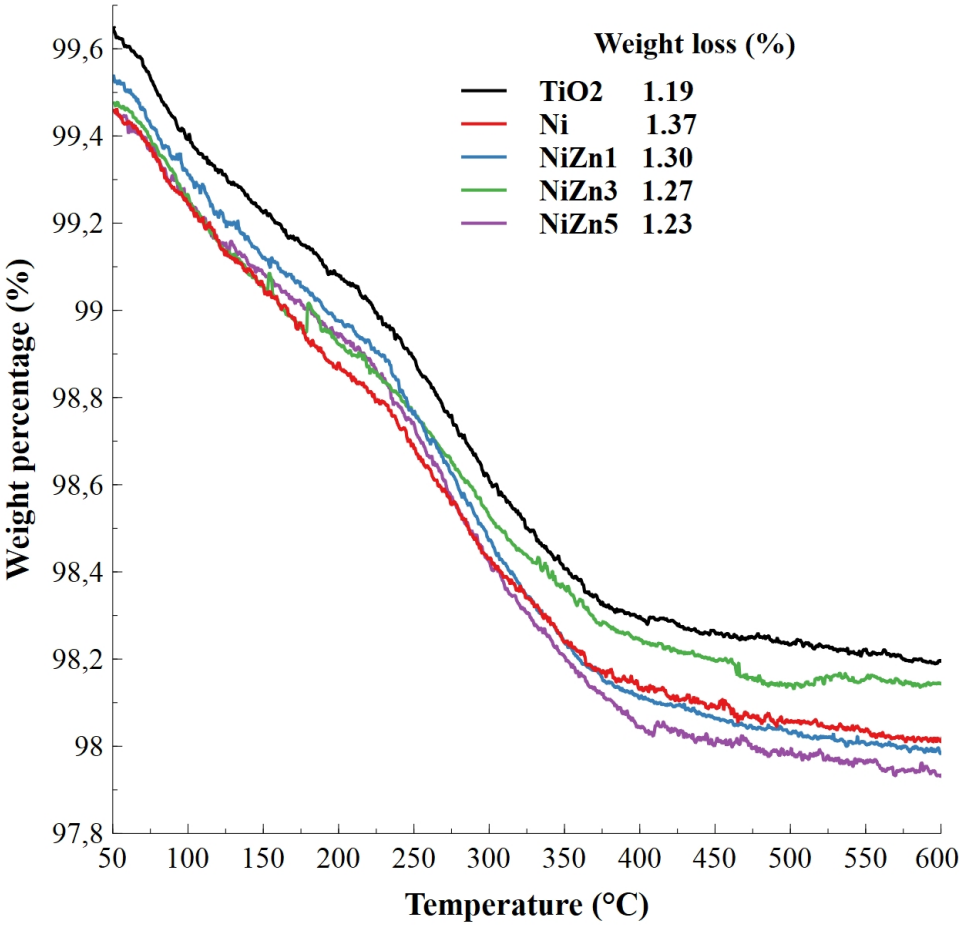

Figure S6: Evolution of the butadiene conversion with time on stream at 20 °C for Ni and NiZn5 catalysts after thermal treatment under H_2 at 200 °C for 1h (20 to 200 °C at 3 °C.min^{-1}) (0.5 wt% Ni) (10 mg of Ni/TiO_2 and 15 mg of NiZn(1:5)/TiO_2 diluted with 90 mg TiO_2). The hatched areas correspond to the periods of treatment under H_2 at 200°C.